Gold-quartz veins in metamorphic terranes and their bearing on the role of fluids in faulting

François Robert

Geological Survey of Canada, Ottawa, Ontario

Anne-Marie Boullier and Karima Firdaous

Centre de Recherches Pétrographiques et Géochimiques, CNRS, Vandoeuvre-les-Nancy, France

Abstract. Gold-quartz vein fields in metamorphic terranes such as greenstone belts provide evidence for the involvement of large volumes of fluids during faulting and may be products of seismic processes near the base of the seismogenic regime. In the Val d'Or district of the Abitibi greenstone belt, Canada, quartz-tourmaline-carbonate veins form a vein field (30 x 15 km) in the hanging wall of a crustal-scale fault zone, which was the main channelway for upward migration of the deeply generated fluids. The veins occur in small high-angle reverse faults and in adjacent horizontal extensional fractures extending up to 75 m in intact rocks. They have formed incrementally during active reverse faulting in response to crustal shortening, at depths corresponding to those at the base of the seismogenic zone in actively deforming crust. Detailed structural and fluid inclusion studies provide evidence for generally lithostatic but fluctuating fluid pressures (ΔP_f of the order of 200 MPa) and for cyclic stress reversals during vein formation and provide good support for the fault valve model. A comparison of vein characteristics with "standard" earthquake rupture parameters suggests that each slip increment along veins in reverse faults was accompanied by a small earthquake ($4 > M > 3$ or less). The large vein field thus represents both the extent of fluid dispersion in the hanging wall of a crustal-scale channelway and the distribution of small earthquakes integrated over the lifetime of the hydrothermal system. It is proposed that such small earthquakes along veins in reverse faults are related to large earthquakes ($M > 6$) nucleating near the base of the seismogenic regime along the nearby crustal-scale fault, either as aftershocks or as a precursory smarm.

Introduction

Fault-hosted gold-quartz vein systems in deformed terranes provide good evidence for fluid involvement during faulting, because quartz, gold, and other vein components are tracers for fluid flow [*Kerrich et al.*, 1984; *Kerrich*, 1986]. Their formation is interpreted to involve coupled stress cycling and fluid pressure cycling correlated to the earthquake stress cycle [*Sibson et al.*, 1988; *Cox et al.*, 1990, 1991; *Boullier and Robert*, 1992]. These vein systems may thus be considered as exhumed fossil products of seismic activity and offer the possibility of studying the effects and importance of overpressured fluids along seismically active faults, a subject of considerable interest [see *Rice*, 1992; *Byerlee*, 1993]. Considered at the district scale, these systems may also provide insight on larger-scale fluid circulation and redistribution in the crust accompanying large earthquakes. The main objectives of this paper are to integrate existing and new evidence for stress and fluid pressure cycling during development of gold-quartz vein systems and to explore further potential links between vein formation and earthquake processes and their implications. Potential avenues for future research are also suggested.

Gold-quartz-tourmaline-carbonate-pyrite veins of the Val d'Or district in Late Archean southeastern Abitibi greenstone belt, Canada, have been structurally documented in detail and offer a good opportunity for studying fault-related processes. The veins are well exposed in three dimensions within numerous deep mines (up to 2 km) and they typify the structural character of many other mesothermal gold-quartz vein deposits and districts around the world [*Eisenlohr et al.*, 1989; *Hodgson*, 1989; *Poulsen and Robert*, 1989]. The structural attributes of these gold-quartz veins, constraints from fluid inclusions, and an interpretation of the dynamics of their development are presented and provide a basis for discussion of potential relationships with earthquake processes.

Structural Setting of Gold-Quartz Veins at Val d'Or

Like many other mesothermal gold-quartz vein districts, Val d'Or is localized along a crustal-scale, first-order fault zone, the Larder Lake-Cadillac fault zone (LLCF). The LLCF separates graywacke mudstones of the Pontiac Subprovince to the south from alternating belts of volcanic (~2700 Ma) and sedimentary rocks (<2688 Ma) rocks of southeastern Abitibi Subprovince to the north (Figure 1). The supracrustal rocks in the area have been deformed and intruded by syntectonic to late tectonic intrusions between ~2700 and 2670 Ma [*Feng and Kerrich*, 1991; *Corfu*, 1993]. Three main phases of
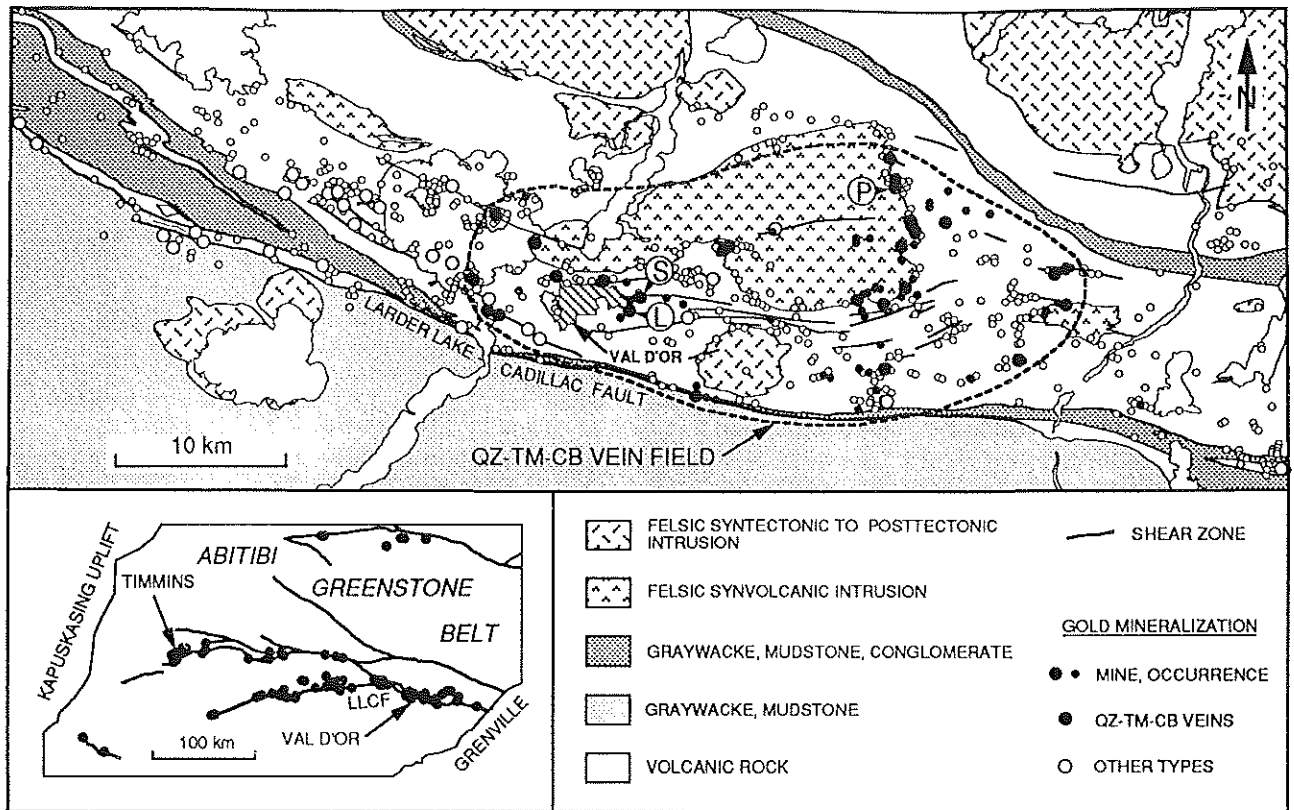
Figure 1. Simplified geological map of the Val d'Or area showing the distribution of different types of known gold deposits and occurrences. Quartz-tourmaline-carbonate veins occur within a restricted area and define an auriferous vein field, outlined by the heavy dashed line. S, Sigma mine; L, Lamaque mine; P, Perron mine. The inset shows the location of the Val d'Or district within the Abitibi greenstone belt, as well as the distribution of major fault zones and spatially associated major gold deposits.

deformation have been documented in the area [*Robert*, 1990]: an early phase of D_1 folding has been recognized locally, especially in the western part of the area (Figure 1). A penetrative E-W subvertical foliation, containing a downdip elongation lineation, overprints such folds and defines a second phase of deformation. D_2 is largely responsible for the dominantly E-W structural trend in the area and records significant N-S shortening across the belt. A third increment of dextral transcurrent deformation was largely localized along the LLCF, at the subprovince boundary.

In addition to the first-order LLCF, which extends over a strike length in excess of 200 km, the Val d'Or district is characterized by the presence of several second-order shear zones, traceable along strike for 1-10 km, and of numerous third-order shear zones, with less than 1 km of strike length. All shear zones are subparallel in strike to the structural trend in the district (Figure 1), but they differ in dip (Figure 2): third-order shear zones dip 35 to 75° north or south; second-order shear zones are subvertical, as constrained by drilling and deep mining; the LLCF dips 60-80°N, as indicated by drilling and deep seismic reflection profiling [e.g., *Green et al.*, 1990]. Structural relations indicate that third-order shear zones, with which the majority of gold-quartz veins are associated, formed during the late stages of the D_2 shortening, prior to the D_3 transcurrent deformation [*Robert*, 1990]. The LLCF and probably several second-order shear zones had a complex history of movement and were reactivated during D_3. However, structural relations further indicate that such first- and second-
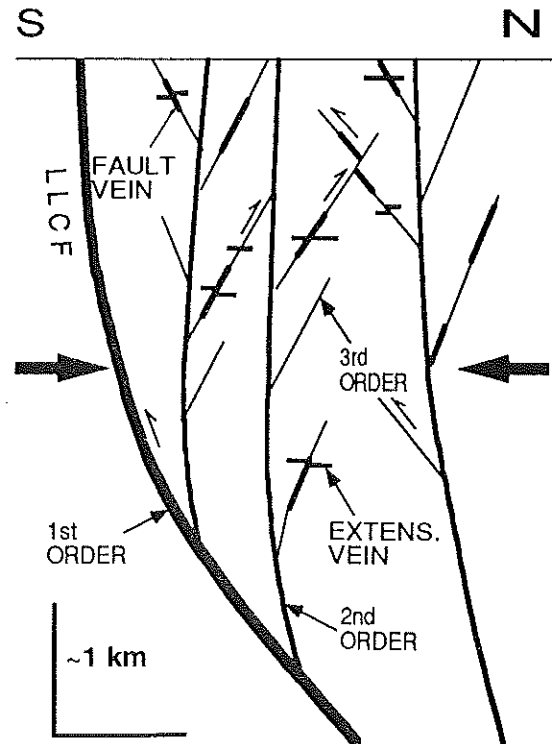

Figure 2. Schematic cross section through the Val d'Or district showing interpreted relationships between veins and shear zones of different orders.

order shear zones were active during the late stages of D_2, at the time of development of third-order shear zones. All documented third-order shear zones are reverse to reverse oblique, and given their moderate to steep dips, the majority of them are high-angle reverse faults [*Robert*, 1990]. Their geometry and kinematics record N-S bulk horizontal shortening (Figure 2), compatible with the regional penetrative D_2 strain and indicating development during crustal shortening.

Peak metamorphism, reached during the late stages of D_2, produced horizontal mineral isograds, indicating lower to middle greenschist grade and yielding pressure estimates of the order of 250-300 MPa, corresponding to about 8-10 km postmetamorphic erosion and uplift [*Carmichael*, 1991], consistent with pressure estimates of 200-250 MPa in a subgreenschist domain west of Val d'Or [*Powell et al.*, 1993]. Shear zones of all orders contain rocks that display mixed brittle-plastic behavior, compatible with the lower to middle greenschist grade of the district. Such fault behavior and metamorphic grade are those expected near the base of the seismogenic regime in actively deforming crust [*Sibson et al.*, 1988].

At Val d'Or, two main generations of shear zone-related gold-quartz veins are recognized [*Robert*, 1994]. Early quartz-carbonate-pyrite veins occur throughout the district but are more abundant in the western part of the district where they are mainly associated with second-order shear zones. They are commonly folded and boudinaged, as a result of overprinting by D_2 deformation, and are cut by diorite and tonalite dikes. The younger quartz-tourmaline-carbonate-pyrite (QTC) veins, which are considered in this paper, are typically associated with third-order shear zones and cut all intrusive rocks of the area. Like their host shear zones, QTC veins formed during the late stages of D_2 shortening and they have been overprinted by significant D_3 transcurrent deformation only within the LLCF [*Robert*, 1990]. Hydrothermal alteration minerals around the veins overprint peak metamorphic assemblages [*Robert and Brown*, 1986a].

All QTC veins possess identical hydrothermal and structural characteristics. They occur within the area outlined in Figure 1 and define a vein field [*Robert*, 1994], approximately 30 x 15 km, which developed during the late stages of D_2 regional shortening. Within this vein field, QTC veins are largely associated with third-order shear zones, but they also occur within the LLCF and second-order shear zones. Such a vein distribution, coupled with structural relations described above, indicates that shear zones of all orders formed a district-scale, three-dimensional network of interconnected shear zones at the time of QTC vein development, as depicted in Figure 2.

Crustal-scale structures such as the LLCF are generally regarded as the main channelways for upward migration of deeply generated fluids [*Eisenlohr et al.*, 1989; *Kerrich and Wyman*, 1990]. Along such structures, the distribution of gold-quartz vein fields or districts likely reflects that of zones of significant upward fluid flow. At the scale of the district, however, the typical distribution of veins in rocks adjacent to crustal-scale structures, as at Val d'Or (Figure 1), can be regarded as representing the extent of fluid "dispersion" around a zone of upward fluid migration along the adjacent first-order structure. The QTC veins at Val d'Or occur only to the north and on the hanging wall side of the LLCF (Figures 1 and 2); such vein distribution is consistent with fluid leakage into the hanging wall of a main conduit along second- and third-order

structures. The presence of abundant tourmaline in these veins indicates that the mineralizing fluids were enriched in boron. Because volcanic rocks hosting the majority of the veins have very low boron contents, the most likely sources of boron are the graywacke mudstones of the Pontiac Subprovince, occurring in the footwall of the LLCF and inferred to underthrust southern Abitibi Subprovince [*Feng and Kerrich*, 1992]. This suggests that mineralizing fluids have reacted with sedimentary rocks below and along the LLCF prior to their dispersion in subsidiary structures within volcanic rocks in its hanging wall.

Structural Characteristics of QTC Veins

Two main types of auriferous veins are particularly well developed among the QTC veins at Val d'Or: shear zone-hosted fault veins and fringing extensional veins. The QTC vein gold deposits themselves are networks of single to multiple sets of fault veins combined with extensional veins. As illustrated in Figure 3, deposits at Val d'Or typically combine one set of fault veins in moderately to steeply dipping shear zones and one set of shallowly dipping extensional veins. The preserved portions of these vein networks have significant vertical extent, as they are exposed down to a depth of nearly 2 km at the Sigma-Lamaque deposit (Figure 3).

The structural characteristics of the QTC veins at Val d'Or have been described in detail by *Robert and Brown* [1986a, b], *Robert* [1990], and *Boullier and Robert* [1992]. Their most significant structural features, together with new documentation, are presented below.

Mesostructures

Fault veins. Fault veins form ellipsoidal lenses (25-100 m long x 1-2 m thick) within more continuous host shear zones or discrete faults (50-1000 m long) and have moderate to steep dips. They are typically laminated, reflecting their incremental development, and consist of individual quartz laminae (1-20 m long x <10 cm thick) separated either by discrete slip surfaces (Figures 4a and 4b) or by slivers of foliated wall rocks of variable thickness [*Robert and Brown*, 1986a; *Robert*, 1990].

Striations on slip surfaces are common and are consistent with the slip directions determined along the host shear zones. Slicken fibers of quartz and tourmaline on slip surfaces present in several deposits further indicate reverse to reverse-oblique movements along the veins, again consistent with those along the host shear zones. These hydrothermal slicken fibers demonstrate that development of fault veins was accompanied by active reverse slip. In a few cases, it can be demonstrated that fault veins occupy releasing bends and dilational jogs along their host shear zones.

Incorporation of foliated wall rock slivers into the veins and the replacement of foliation seams adjacent to veins by hydrothermal minerals clearly indicate that fault veins developed within existing shear zones [*Robert and Brown*, 1986a]. The consistency of direction and sense of slip along fault veins with those along the host shear zones further indicates that the shear zones were still active as high-angle reverse faults at the time of vein formation.

The total amount of reverse slip along fault veins and their host structures could be determined in a small number of cases: it ranges from 0.1-2.0 m for shear zones of 25-100 m dip
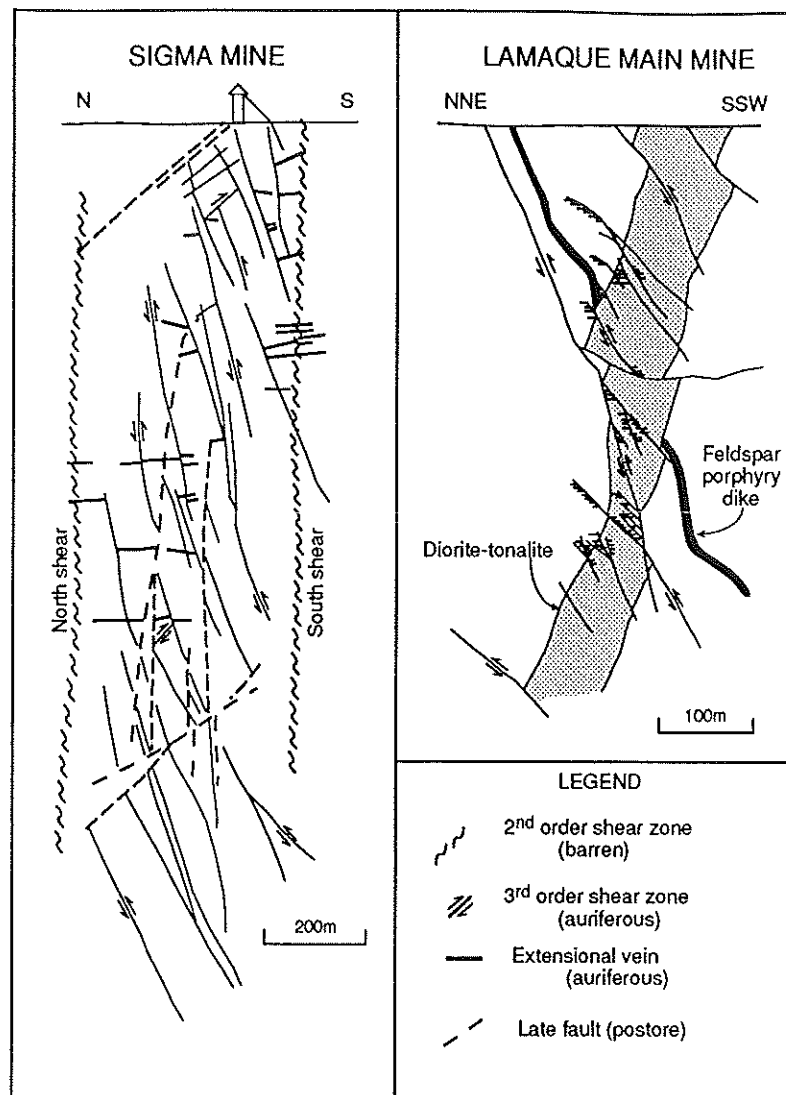
Figure 3. Simplified vertical cross-sections through quartz-tourmaline-carbonate vein networks of the Sigma and Lamaque deposits, adapted from *Robert and Brown* [1986a] and *Wilson* [1948], respectively. Note the difference in scale. In both cases, the networks comprise moderately to steeply dipping shear zones and contained fault veins and fringing subhorizontal extensional veins.

length (F. Robert, unpublished data, 1993) to 20-30 m along shear zones in excess of several hundred meters of dip length, as illustrated in Figure 3 by the offset of the preore tonalite along reverse shear zones at the Lamaque mine. Such figures are probably maximum values for the amount of slip related to vein formation, because they include slip along the host shear zone or fault prior to vein development. It is important to note that hydrothermal slicken fibers (quartz and tourmaline) indicating normal movement are also observed on a small number of fault veins.

In addition, two types of breccia locally occur along or within fault veins. The first type is a jigsaw puzzle consisting of unrotated angular wall rock fragments set in a hydrothermal matrix of fine grained massive tourmaline (Figure 4c). The second can be regarded as a fault breccia: it forms narrow elongate lenses within some fault veins and consists of angular but rotated fragments of veins and altered wall rocks set in a hydrothermal matrix of quartz or tourmaline. The presence of the same hydrothermal minerals in the breccia

matrices as in fault veins indicates that brecciation was an integral part of vein development rather than having formed at a later time.

Extensional veins. Two main types of extensional veins are observed. The more common planar extensional veins form subhorizontal tabular bodies extending into intact rocks up to 75 m away from, and on both sides of, fault veins with which they are spatially associated. These veins maintain their subhorizontal orientation throughout the district and over a considerable vertical interval, as at the Sigma mine (Figure 3). They have high aspect ratios, covering areas of 10^2-10^4 m^2 with thicknesses ranging from 1 cm to 1 m. Extensional veins generally consist of several wall-parallel ribbons of varying mineral proportions and textures (Figure 4d), representing growth layers and attesting to their incremental development. Individual ribbons commonly display well-developed open-space filling textures or mineral fibers (tourmaline ± carbonate; Figure 4d) and crack seal structures; they reach thicknesses of 10 cm and areas of 1000
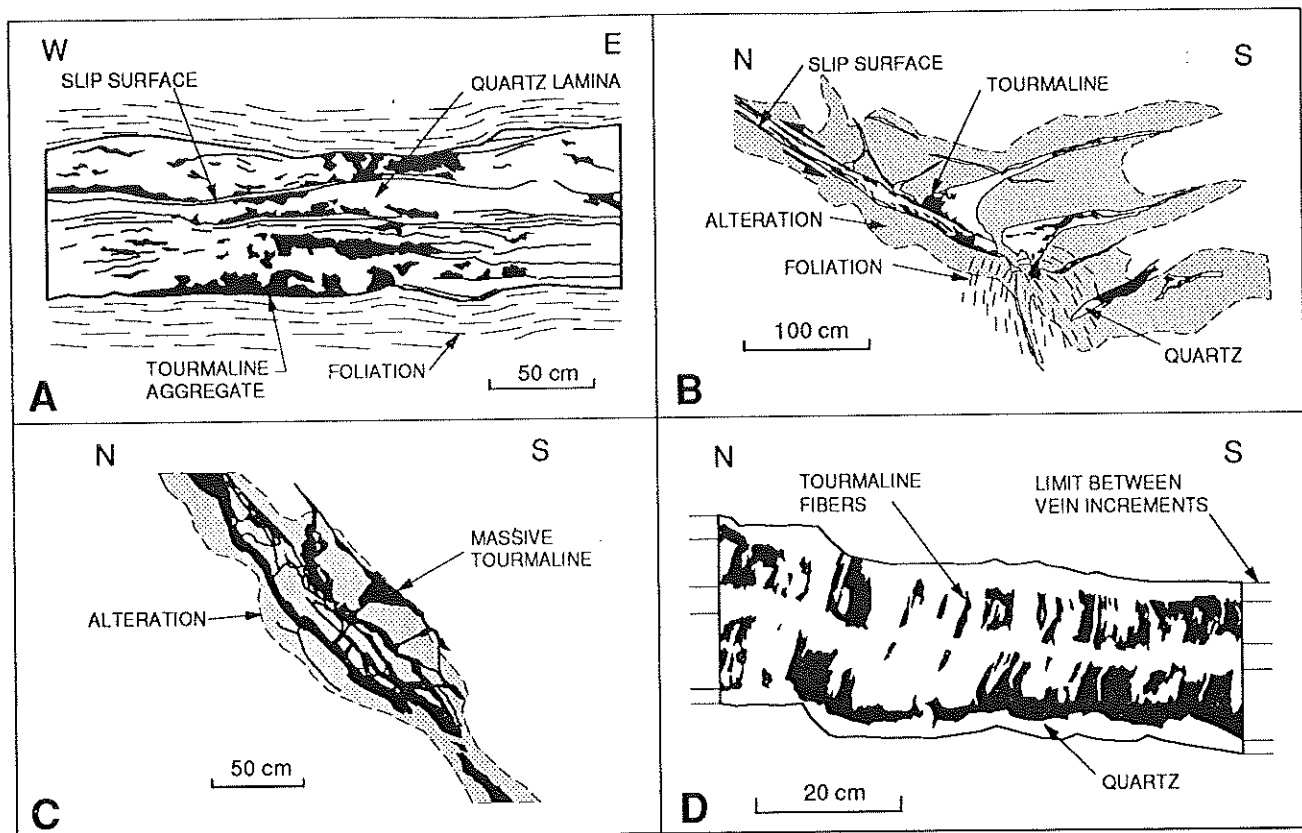
Figure 4. Examples of QTC veins, traced from photographs. (a) Horizontal plan view of a fault vein with abundant slip surfaces; the "clean" quartz lamina in the center of the vein represents a late increment of opening. (b) Vertical cross section of downdip termination of a reverse fault vein with related sigmoidal extensional veins. Truncated extensional veins likely formed during an earlier increment of fault vein propagation. (c) Vertical cross section of a jigsaw puzzle breccia consisting of angular altered wall rock fragments in a massive fine-grained tourmaline matrix. (d) Vertical cross section of a subhorizontal extensional vein with well-developed vertical tourmaline fibers; note the presence of multiple increments of vein growth.

m^2. Lack of offsets of markers other than those that can be accommodated by pure dilation, the orientation of mineral fibers perpendicular to vein walls (Figure 4d), and the common presence of rock bridges show that these veins occupy true extension fractures.

Sigmoidal extensional veins of restricted lateral extent are also locally developed near the edges of reverse fault veins: they occur more specifically on the footwall side at updip fault vein terminations, as represented in the cross section of the Lamaque mine (Figure 3), and on the hanging wall side at downdip fault vein terminations (Figure 4b). These veins are interpreted to represent tensile fractures, or "wing cracks," developed at fault tips [see *Pollard and Segall*, 1987; *Scholz*, 1989]: their common position at fault vein terminations and their sigmoidal shapes are consistent with reverse faulting. Such sigmoidal extensional veins are distinguished from the throughgoing planar extensional veins described above: planar extensional veins, where not offset by subsequent reverse slip, extend on both sides of a single fault vein in intact rocks and pinch away from it, in contrast to sigmoidal extensional veins which are clearly restricted to one side of the fault (Figure 4b). In addition, small extensional veins parallel to the shear zone foliation locally occur adjacent to fault veins, indicating local extensional opening of the foliation planes, consistent with crack seal textures parallel to walls of quartz laminae locally present within fault veins.

Mutually crosscuting relationships are observed between fault veins and planar extensional veins, commonly along the same fault vein and locally at a single site [see *Robert and Brown*, 1986a]. Such relationships indicate that the two vein types are broadly contemporaneous and developed in a cyclic, sequential manner [*Robert*, 1990; *Boullier and Robert*, 1992]. The presence of hydrothermal slicken fibers and sigmoidal extensional veins at fault vein terminations further indicates that vein development accompanied active reverse faulting.

Microstructures

Microstructures of both types of veins have been examined in detail by *Boullier and Robert* [1992] and reflect the interplay of stages of vein growth and vein deformation in both vein types (Table 1). Growth microstructures are best preserved in tabular extensional veins extending outside shear zones into undeformed wall rocks, whereas fault veins are dominated by deformation microstructures consistent with their development in active faults.

In extensional veins, growth microstructures include open-space filling, mineral fibers and crack seal structures, the latter

Table 1. Summary of Vein Microstructures and Their Significance

	Fault Vein		Extensional Vein	
Growth features		open-space filling crack seal (rare)	*vertical dilation*	open-space filling crack seal mineral fibers horizontal FI planes
Deformation features	*aseismic slip*:	stylolites plastic deformation dynamic recrystallization	*vertical shortening*	kinked fibres vertical FI planes horizontal boudinage
	seismic slip (?):	FI planes slip planes crushed tourmaline		

FI plane is fluid inclusion plane

two recording vertical dilation corresponding to opening of the veins (Table 1). Individual ribbons or segments of ribbons are dominated by one of these three growth structures, and it is postulated that the type of microstructure produced reflects differences between the rate of wall separation and that of mineral precipitation, as proposed by *Cox* [1991] and *Foxford et al.* [1991]. In addition to undulose extinction and prismatic subgrains in quartz, deformation microstructures include kinks developed in mineral fibers and crystals at high angle to vein walls, as well as stretching of crystals parallel to vein walls [*Boullier and Robert*, 1992]. Such deformation microstructures reflect increments of vertical shortening of the extensional veins.

In fault veins, the only observed growth features within individual quartz laminae are rare crack seal structures [see *Boullier and Robert*, 1992, Figure 9a] and more common open-space filling textures (Table 1). Deformation microstructures dominate, and those produced by dynamic recrystallization of quartz (prismatic subgrains, polygonized grains) are the most common. However, adjacent quartz laminae may display contrasting degrees of strain: laminae with completely recrystallized quartz can be juxtaposed against laminae containing large undeformed quartz crystals, as illustrated in Figure 5. Stylolites are also commonly developed along the walls of laminae; the N-S, horizontal orientation of their peaks is consistent with the maximum principal stress direction at the time of vein development (Figure 2). In addition, discrete bands of very fine grained crushed tourmaline crystals (size < 5 μm) developed within tourmaline-rich layers and corresponding to slip surfaces are commonly present.

Healed microcracks, outlined by planes of fluid inclusions occur with systematic orientations in both vein types. As reported by *Boullier and Robert* [1992], such microcracks are of mode I, and their different orientations within a given vein must reflect different orientations of the local stress field at different times. As shown in Figure 6a, healed microcracks in an extensional vein at the Perron deposit are oriented both parallel and perpendicular to the vein walls, indicating episodes of vertical dilation and vertical shortening, respectively. In a shallow dipping segment of a fault vein within the same deposit, microcracks have similar orientations relative to the vein walls (Figure 6b). Microcrack orientations in the extensional vein from the Perron deposit are very similar to those determined in extensional veins at the Sigma and New Pascalis deposits [*Boullier and Robert*,

1992] occurring in different parts of the district (Figure 1). This shows that the systematic orientations of healed microcracks, at least within extensional QTC veins, are not due to special local conditions but are a normal consequence of the vein development process.
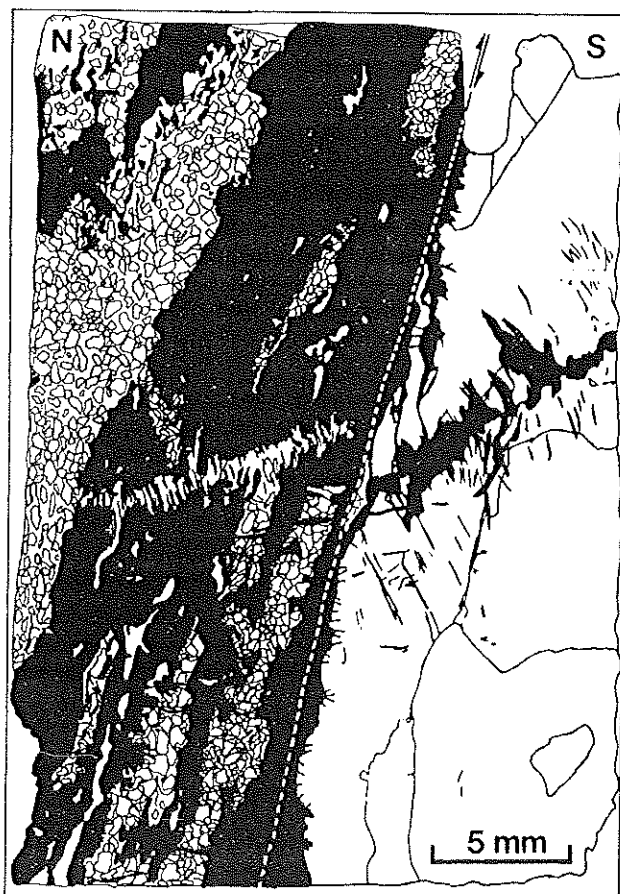

Figure 5. Line drawing from a thin section (oriented vertically and looking east) of a fault vein from the Sigma mine, showing the contrast in strain between two adjacent quartz (-tourmaline) laminae, separated by a very thin slip surface (white dotted line). The lamina on the left consists of tourmaline (black) and completely recrystallized quartz (small white grains), whereas the lamina on the right contains large subhedral quartz grains (white) that are nearly undeformed, with some tourmaline (black). Thin section is 2 cm wide.
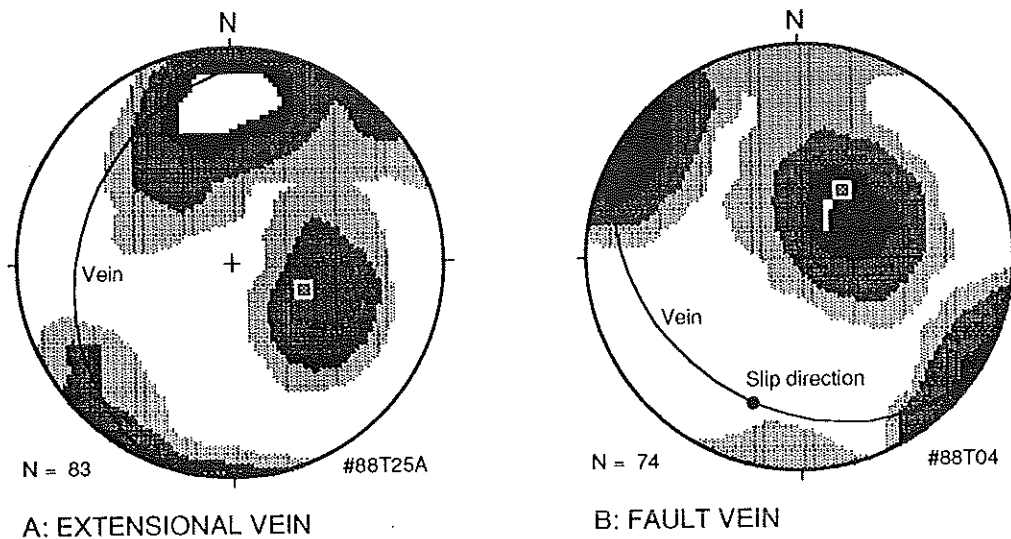
A: EXTENSIONAL VEIN   B: FAULT VEIN

Figure 6. Stereographic projections (equal area) of poles of secondary fluid inclusion planes; Perron mine. Kamb contours. In both types of veins, planes are oriented parallel and perpendicular to the vein walls.

Significant variations in the degree of plastic deformation and in the abundance of microcracks are observed between adjacent ribbons in extensional veins and between adjacent quartz laminae in fault veins (Figure 5). Truncations of "old" microcracks by newly added material, showing little or no evidence of plastic deformation, are also observed in both vein types. These observations indicate that stages of vein growth alternated with stages of vein deformation, and that both stages are part of a repeating cycle leading to the development of ribboned extensional and laminated fault veins [*Boullier and Robert*, 1992]. They also verify that the observed deformation of vein materials is not the result of superimposed postvein strain.

Significance of Vein Structures

Structural features of QTC veins presented above provide insights on three important aspects of their formation, which are emphasized here to provide a basis for subsequent discussions.

First, fault veins clearly developed as a result of active reverse slip along shear zones and faults that were moderately to severely misoriented relative to the prevailing stress field (Figure 2). As pointed out by *Sibson et al.* [1988], for typical coefficients of rock friction, slip along such faults is only possible under high P_{fluid} conditions. Given their consistent subhorizontal orientations throughout the vein field and over a significant vertical interval, their development in intact rocks in a compressional stress field (Figure 2), and their inferred depth of formation, planar extensional veins are best interpreted as hydraulic fractures and provide good evidence for the existence of overpressured fluids. As argued by a number of authors, tensile fracturing at the depths considered here requires fluid pressures exceeding the minimum (vertical in this case) principal compressive stress [e.g., *Secor*, 1965, 1969; *Etheridge et al.*, 1984]. Within a large number of ribbons within planar extensional veins, the presence and preservation of open-space filling textures such as large scheelite crystals and rosettes of tourmaline crystals up to 10 cm long indicate that the rate of fracture wall separation was

greater than the rate of crystal growth and that the fracture was at least partly opened until complete filling [*Robert and Brown*, 1986b], requiring P_f at least equal to lithostatic load.

Furthermore, the presence of small extensional veins parallel to shear zone foliation and of crack seal structures parallel to quartz laminae within fault veins indicates extensional opening of weak planes (lower tensile strength than adjacent intact rocks) oriented at high angle to the maximum principal compressive stress and is also consistent with hydraulic fracturing, as discussed by *Gratier* [1987]. Finally, the fact that tabular extensional veins are spatially associated with shear zones and taper away from them indicates that the shear zones themselves are the sources of the overpressured fluids.

Second, the mutually crosscutting relationships among extensional and fault veins attest to their sequential development in a repeating cycle. The juxtaposition of material of contrasting degree of strain and the truncation of old cracks by newly deposited material further indicate that alternating stages of growth and deformation in both vein types are also part of this cycle.

Finally, deformation structures within fault veins record contrasting deformation processes, commonly juxtaposed within single thin sections (Table 1). Stylolites and recrystallized quartz grains indicate aseismic (low strain rate), fluid-enhanced deformation [*Gratier and Gamond*, 1989], attributed to horizontal shortening and vertical elongation. On the other hand, discrete slip surfaces defined by very fine grained crushed tourmaline, as well as jigsaw puzzle and fault breccias adjacent to fault veins likely indicate high strain rate deformation, perhaps associated with seismic slip, though additional work is needed to substantiate this inference.

Fluid Inclusion Constraints

Fluid inclusions in fault-related veins such as those described here provide direct information on the nature of the fluids infiltrating faults (e.g., local pore fluid versus external fluid). In addition, fluid inclusions have been successfully used in a number of studies to document and to place constraints on

fluid pressure variations during faulting [e.g., *Parry and Bruhn*, 1990]. A detailed fluid inclusion study of auriferous QTC veins from three deposits of the Val d'Or district is presently underway to document fluid evolution in relation to the complex structural evolution of the veins and to verify the presence of fluid pressure variations during vein development. Here we present the most relevant results from the Sigma mine, where our work is most advanced and where aspects of fluid inclusions have also been previously studied by *Robert*

and Kelly [1987] and *Guha et al.* [1991]. Microthermometric data are reported here for one sample of a fault vein and two of neighboring extensional veins, and are presented in Figure 7.

Thermometric data were interpreted in terms of composition and density of the trapped fluids based on work by *Swanenberg* [1979], *Jacobs and Kerrick* [1981], and *Heyen et al.* [1982] for the composition and density of the carbonic phase of H_2O-CO_2 inclusions; *Chen* [1972], *Bozzo et al.* [1975], and *Collins* [1979] for the salinity of the aqueous phase in H_2O-
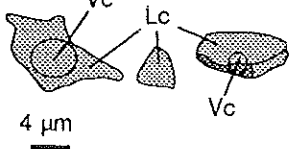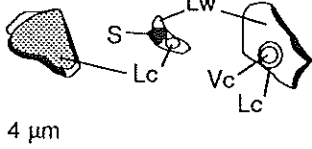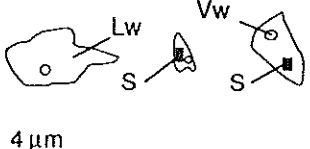
Sample	CO_2 fluid inclusions	H_2O-CO_2 fluid inclusions	H_2O-NaCl fluid inclusions
	4 μm	4 μm	4 μm
89RAO35 Fault vein	Abundance: 75% T_mCO_2 = -58.1 to -57°C T_hCO_2 (L or V) = -27.5 to +28.2°C Density = 520 to 1000 kg/m³	Abundance: 10% Vol% CO_2 = 20-85% T_mCO_2 = -58.3 to -56.8°C T_hCO_2 (L) = +11.5 to +29.9°C T_{mi} = -3.2 to -5.4°C T_{mc} = +7.2 to +8.8°C TH (L or V) = 237 to 320°C TD = 260 to 340°C Salinity = 1 to 4 wt % NaCl eq. Density = 670 to 990 kg/m³	Abundance: 15% T_e = -61.8 to -43.7°C T_{mi} = -46.4 to -3.2°C T_h (L) < 160°C T_{ms} = 177 to 204°C TD = 179 to 220°C Salinity = 5 to 31 wt % NaCl eq. Density = 940 to 1260 kg/m³
89RAO42 Extensional vein	Abundance: 33% T_mCO_2 = -63 to -56.9°C T_hCO_2 (L) = -49.2 to +24.7°C Density = 600 to 1020 kg/m³	Abundance: 33% Vol% CO_2 = 10-85% T_mCO_2 = -63.7 to -56.8°C T_hCO_2 (L) = -49.2 to +24.7°C T_{mi} = -6.2 to -2.9°C T_{mc} = +6.4 to +14.7°C TD = 202 to 335°C Salinity = 2 to 6 wt % NaCl eq. Density = 600 to 1000 kg/m³	Abundance: 33% T_e = -79 to -45°C T_{mi} = -51.2 to -2.4°C T_h (L) < 180°C and >180°C T_{ms} = 163.6 to 189.9 °C Salinity = 4 to 30 wt % NaCl eq. Density = 580 to 1200 kg/m³
89RAO44 Extensional vein	Abundance: 15% T_mCO_2 = -57.1 to -56.7°C T_hCO_2 (L) = -8.7 to +28.8°C Density = 600 to 1030 kg/m³	Abundance: 80% Vol% CO_2 = 15-85% T_mCO_2 = -57.3 to -56.7°C T_hCO_2 (L) = -10.2 to +30.9°C T_{mi} = -10.7 to -0.2°C T_{mc} = +6.5 to +9.9°C T_{ms} = 98 to 232°C TD = 265 to 398°C TH (L or V) = 211 to 425°C Salinity = 3 to 6 wt % NaCl eq. Density = 470 to 1000 kg/m³	Abundance: 5% T_e = -38 to -32.8°C T_{mi} = -8.3 to -1°C T_h (L) < 180°C Salinity = 1.7 to 12 wt % NaCl eq. Density = 950 to 1010 kg/m³

Figure 7. Synthesis of microthermometric fluid inclusion data from three samples from the Sigma mine (Val d'Or). T_mCO_2, melting temperature of the carbonic phase. T_hCO_2 (L or V), homogenization temperature of the carbonic phase to the liquid (L) or to the vapor (V). T_{mc}, melting temperature of the clathrate. TD, decrepitation temperature. TH (L or V), total homogenization to the liquid (L) or to the vapor (V) phase. T_e, temperature of the eutectic. T_{mi}, melting temperature of ice or of salt hydrate. T_{ms}, melting temperature of the daughter mineral. T_h (L), homogenization to the liquid (L) phase. L_c, liquid CO_2. V_c, vapor CO_2. L_w, liquid water. V_w, vapor water. S, daughter mineral.

CO_2 inclusions; *Vanko et al.* [1988] and *Williams-Jones and Samson* [1990] for salt determinations in H_2O-salt inclusions; *Crawford* [1981] and *Zhang and Frantz* [1987] for calculation of $CaCl_2$ wt % in H_2O-salt inclusions; *Potter and Clynne* [1978] and *Bodnar* [1993] for the NaCl-equivalent salinity of H_2O-salt inclusions; and *Zhang and Frantz* [1987] for the density of H_2O-salt inclusions.

Fluid Inclusion Types and Modes of Occurrence

As initially recognized by *Robert and Kelly* [1987], three compositional types of fluid inclusions are present in quartz (Figure 7): CO_2-rich, H_2O-CO_2, and H_2O-NaCl fluid inclusions. All three types of inclusions are present in all veins but they vary in relative abundance from one vein type to the other; CO_2-rich fluid inclusions are more abundant in fault veins than in extensional veins (see Figure 7).

Fluid inclusions show three modes of occurrence in quartz: these are, in order of decreasing importance, in the healed microcracks referred to above, in three-dimensional clusters, and along grain boundaries in plastically deformed quartz. Depending on the degree of plastic deformation of the host crystal, fluid inclusions may show different degrees of reworking. Fluid inclusions in healed microcracks are secondary relative to the host crystal, but as indicated above and discussed in detail by *Boullier and Robert* [1992], the development of these microcracks and the trapping of the fluids is considered to be an integral part of the cyclic development of the veins. All three types of fluid inclusions may occur in healed microcracks. Fluid inclusions scattered in isolated three-dimensional clusters, which are less common, can be considered as primary inclusions. Such clusters consist either of H_2O-CO_2 inclusions with relatively constant degree of filling or of coexisting CO_2-rich fluid inclusions and H_2O-CO_2 inclusions with variable degrees of filling, indicative of reworking of H_2O-CO_2 inclusions by plastic deformation.

In all extensional veins examined to date, healed microcracks contain different fluid inclusion types depending on their orientations: CO_2-rich and H_2O-CO_2 fluid inclusions occur chiefly in subhorizontal planes, parallel to the vein walls, whereas H_2O-NaCl fluid inclusions occur in subvertical planes, perpendicular to the vein walls [*Boullier and Robert*, 1992]. Current investigations indicate that a few subvertical H_2O-NaCl fluid inclusion planes represent the latest microfractures in the rocks. In fault veins, the separation of fluid inclusion types in microcracks of different orientations is not as pronounced.

Microthermometric Data and Fluid Composition and Densities

Fault vein. The fault vein sample considered here (89RAO35) has been described by *Boullier and Robert* [1992, Figures. 5a and 12b]. It is dominated by CO_2-rich fluid inclusions (see Figure 7) which occur both along healed microfractures and as three-dimensional clusters. CO_2-melting temperatures (T_mCO_2) below that of pure CO_2 (Figure 8a) indicate the presence of other volatile components, identified as CH_4 and N_2 by preliminary Raman analyses, consistent with the results of *Robert and Kelly* [1987] and *Guha et al.* [1991] on similar fluid inclusions. Homogenization temperatures of CO_2 (T_hCO_2) range from -27.5°C to +28.2°C (Figure 8b). The peak of T_hCO_2 at approximately +25°C

corresponds to fluid inclusions in planar microcracks which have not been reworked by subsequent plastic deformation. Most fluid inclusions in isolated clusters homogenize to the liquid phase over the entire range shown in Figure 8, and some inclusions homogenize to the vapor phase between +12.3 and +27.5°C. In many cases, such clusters correspond to reworked larger (primary?) inclusions and to plastically deformed healed microcracks, which probably accounts for the scatter of T_hCO_2 and homogenization to the vapor phase. Calculated densities for CO_2-rich inclusions homogenizing to the liquid phase range from 520 to 1000 kg/m^3, and inclusions in planar microcracks $(T_hCO_2 = 25°C)$ have densities of the order of 500-600 kg/m^3.

In this sample, H_2O-CO_2 fluid inclusions are generally scattered in three-dimensional clusters in which the degree of filling varies between 20 and 85 vol % CO_2 (Figure 7). Their volatile component is similar in composition to that of the CO_2-rich fluid inclusions, as indicated by the same range of T_mCO_2 values (Figure 8a), and it contains on average $2\%(CH_4+N_2)$, as determined by graphical methods. However, T_hCO_2 of H_2O-CO_2 inclusions range between +10 and +30°C (Figure 8b), and homogenization is to the liquid phase in all cases. The aqueous phase in H_2O-CO_2 fluid inclusions has a salinity of 1-4 wt % eq NaCl, as determined from the melting temperatures of both ice and clathrate (Figure 7). In the absence of Raman analyses of the volatile phase, bulk densities of H_2O-CO_2 inclusions were only calculated for inclusions in which the volatile phase consists of relatively pure CO_2, i.e., for those containing $2\%(CH_4+N_2)$ or less. Densities calculated from graphical methods range from 670 to 990 kg/m^3.

H_2O-NaCl fluid inclusions only occur along healed microfractures. Low eutectic temperatures (-62°C to -43°C) indicate that other salts are present in addition to NaCl [*Robert and Kelly*, 1987]. Scanning electron microscopy (SEM) investigations of opened fluid inclusions reveal the presence of $CaCl_2$ crystals in some inclusions. Melting temperatures of ice and salt hydrate (T_{mi}) range from -46.4°C to -3.2°C (Figure 8c), indicating total fluid salinity ranging from 5 to 31 wt % eq NaCl. Homogeneization temperatures (to the liquid phase) are generally below 160°C (Figure 8c); in three fluid inclusions, melting temperatures of the contained salt mineral are above the homogeneization temperature $(T_{ms} = 177°C$ to 204°C). As shown in Figure 8c, fluid inclusions in a single microcrack have a narrow range of T_{mi}, indicating a narrow range of salinity, which varies from one microcrack to the other. Homogenization temperatures of fluid inclusions within a microcrack may be similar or may show a significant scatter (Figure 8c). Calculated densities for microcracks in which fluid inclusions have a narrow range of T_h vary from 940 to 1260 kg/m^3.

Extensional veins. The two extensional vein samples considered here show contrasting proportions of fluid inclusion types (Figure 7), as well as some differences in their compositions. Sample 89RAO42 is from a quartz-tourmaline vein showing multiple growth layers [*Boullier and Robert*, 1992, Figures 4c and 6a-6c] and contains approximately equal proportions of the three types of fluid inclusions (CO_2-rich, H_2O-CO_2, and H_2O-NaCl). Sample 89RAO44 is from a neighboring massive quartz vein in which H_2O-CO_2 inclusions dominate (Figure 7).

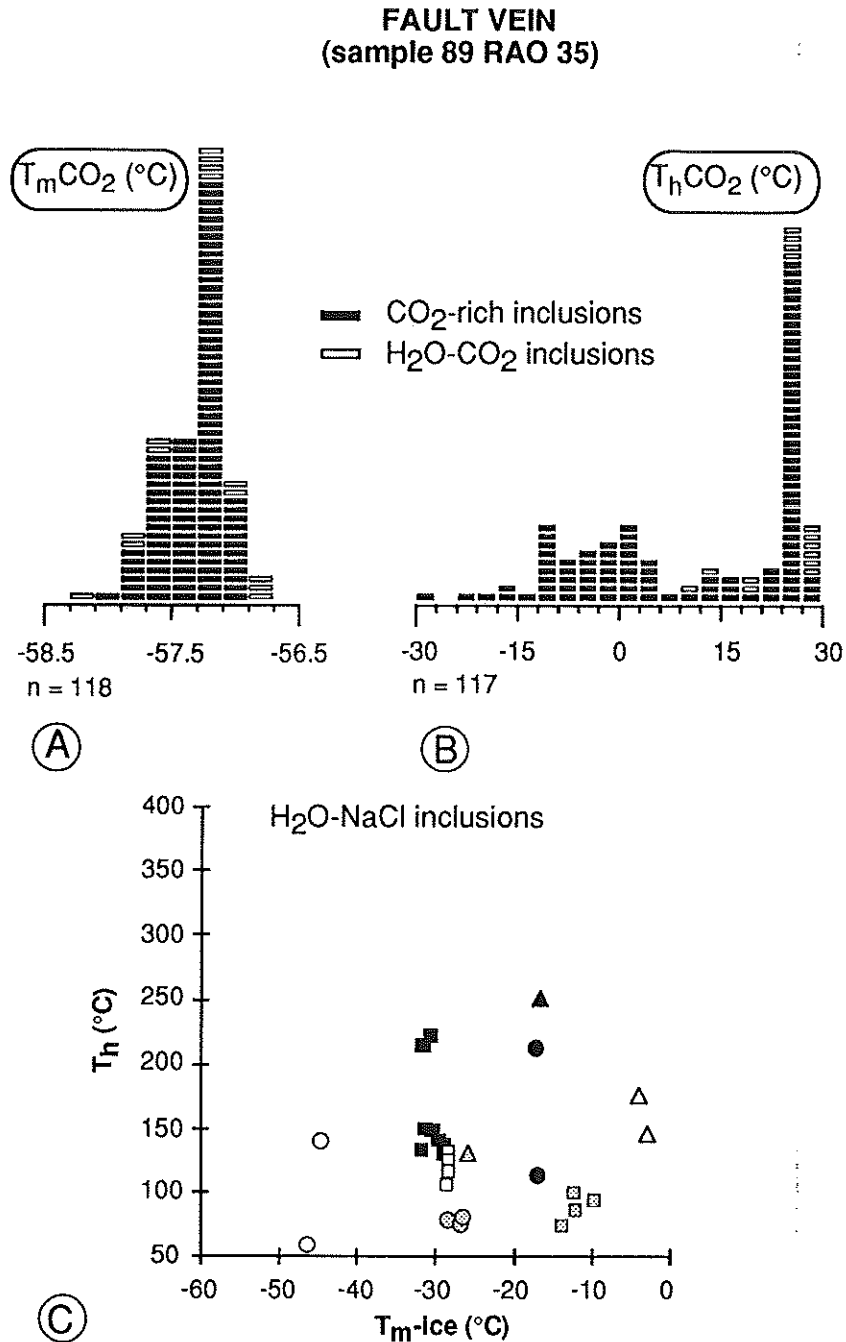In both samples, CO_2-rich and H_2O-CO_2 fluid inclusions occur in clusters and in healed microfractures which are parallel

**FAULT VEIN
(sample 89 RAO 35)**

Figure 8. Fluid inclusion data, fault vein sample 89 RAO 35. (a) Histogram of T_mCO_2 for both CO_2-rich and H_2O-CO_2 fluid inclusions. (b) Histogram of T_hCO_2 for both CO_2-rich and H_2O-CO_2 fluid inclusions. (c) T_h versus T_{mi} of H_2O-NaCl fluid inclusions; measurements in different fluid inclusion planes represented by different symbols. Terminology as defined in Figure 7 caption.

to the vein walls. CO_2-rich and CO_2-H_2O fluid inclusions have the same ranges of T_mCO_2 and T_hCO_2, but this range is narrower in sample 89RAO44 than in sample 89RAO42 (Figures 9a and 10a). The T_mCO_2 below -56.6°C indicate the presence of volatile components other than CO_2, considered to be CH_4 and N_2 by analogy with fluid composition in sample 89RAO35 and based on the results of *Guha et al.* [1991]. However, the volatile phase in a large number of CO_2-rich and H_2O-CO_2 inclusions in sample 89RAO44 contains nearly pure

CO_2 (Figure 10). Calculated densities of such pure CO_2-rich fluid inclusions range from 600 to 1030 kg/m³.

The degree of filling of H_2O-CO_2 inclusions is also variable, and it ranges from 10 to 85 vol % CO_2 within the samples and among inclusions within a single cluster or microcrack (Figure 7). Despite such variations in T_hCO_2 and degree of filling of H_2O-CO_2 inclusions within single microfractures, T_mCO_2 (Figure 9c) and T_{mc} are relatively constant, suggesting that a homogeneous H_2O-CO_2 fluid was
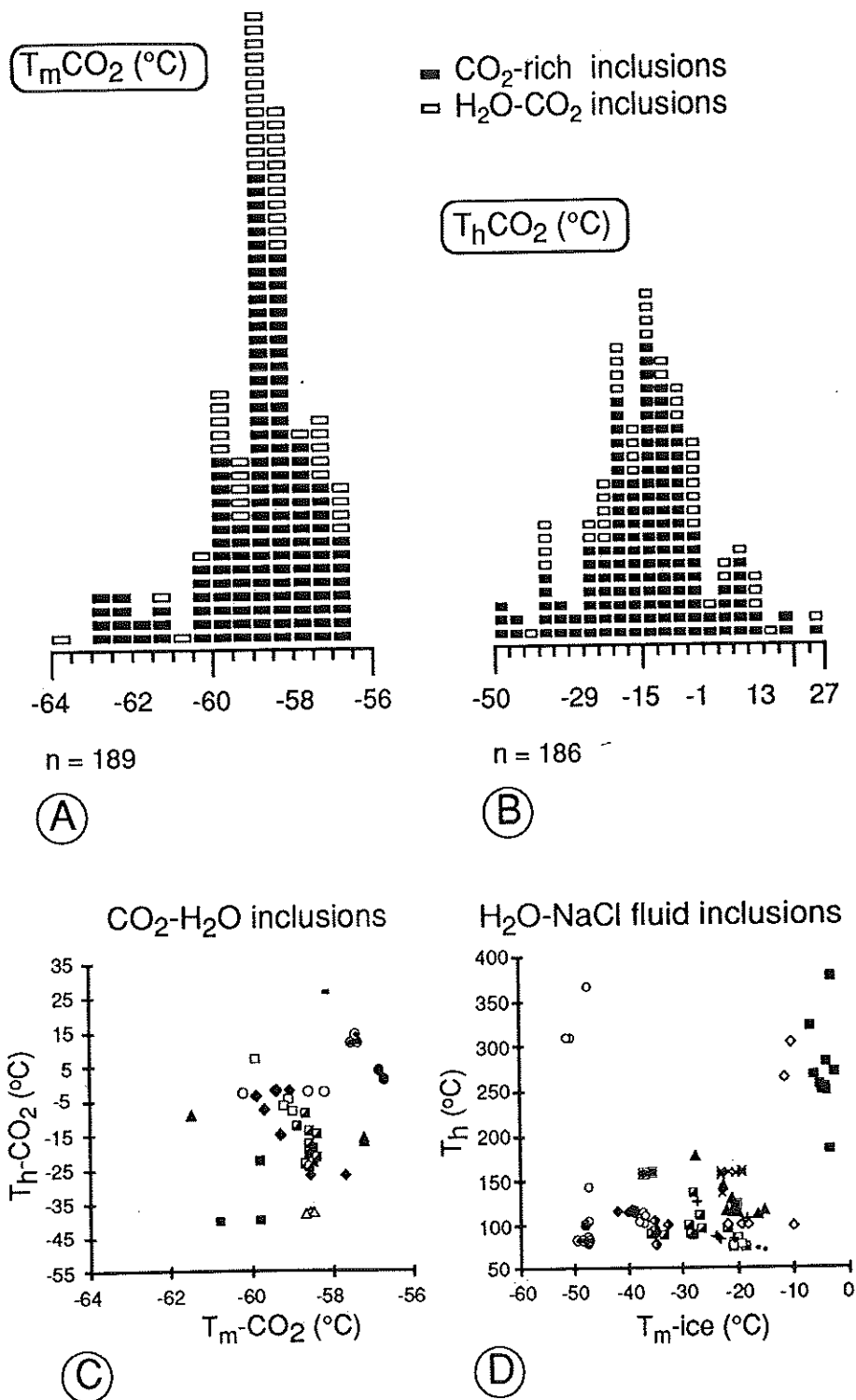
EXTENSIONAL VEIN
sample 89RAO42

Figure 9. Fluid inclusion data, extensional vein sample 89 RAO 42. (a) Histogram of T_mCO_2 for both CO_2-rich and H_2O-CO_2 fluid inclusions. (b) Histogram of T_hCO_2 for both CO_2-rich and H_2O-CO_2 fluid inclusions. (c) T_hCO_2 versus T_mCO_2 in H_2O-CO_2 fluid inclusions; measurements in different fluid inclusion planes represented by different symbols. (d) T_h versus T_{mi} in the H_2O-NaCl fluid inclusions; measurements in different fluid inclusion planes represented by different symbols. Terminology as defined in Figure 7 caption.
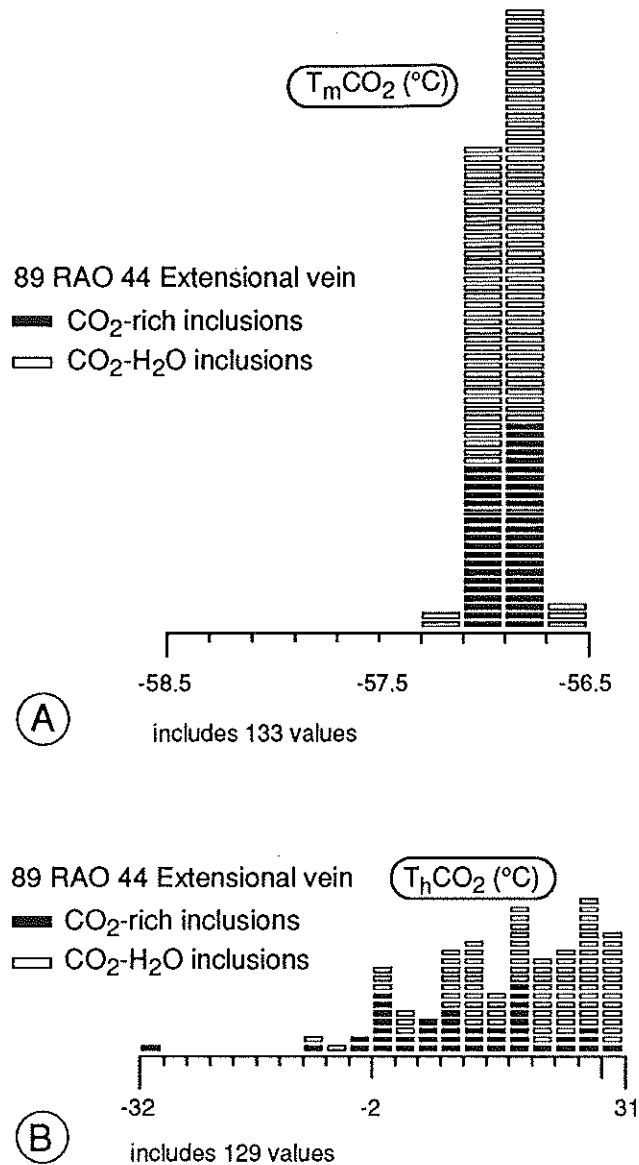
T_mCO_2 (°C)

89 RAO 44 Extensional vein

▬ CO_2-rich inclusions

▭ CO_2-H_2O inclusions

-58.5   -57.5   -56.5

(A)   includes 133 values

89 RAO 44 Extensional vein T_hCO_2 (°C)

▬ CO_2-rich inclusions

▭ CO_2-H_2O inclusions

-32   -2   31

(B)   includes 129 values

Figure 10. Fluid inclusion data, extensional vein sample 89RAO 44. (a) Histogram of T_mCO_2 for both CO_2-rich and H_2O-CO_2 fluid inclusions. (b) Histogram of T_hCO_2 for both CO_2-rich and H_2O-CO_2 fluid inclusions. Terminology as defined in Figure 7 caption.

initially trapped in these microfractures and was subsequently modified. The melting temperatures of clathrate (T_{mc}) in H_2O-CO_2 inclusions (Figure 7) indicate the presence of salt in the aqueous phase. In sample 89RAO42, T_{mc} values above 10°C reflect the presence of CH_4 and other volatiles. Considering inclusions with T_mCO_2 close to that of pure CO_2, the calculated salinities of the aqueous phase fall in the range of 2 to 6 wt % eq NaCl in both samples. Upon heating, H_2O-CO_2 inclusions generally decrepitate between 200 and 400°C (Figure 7); total homogenization temperature (TH) determined on a number of inclusions range from 270 to 280°C in sample 89RAO42 and from 212 to 425°C in sample 89RAO44. Total homogenizations to both the liquid and the vapor phases have been observed in each sample. Estimated densities for fluid inclusions in which the volatile phase is composed of nearly

pure CO_2 are 600-1030 kg/m³ for sample 89RAO42 and 470-1000 kg/m³ for sample 89RAO44 (Figure 7).

H_2O-NaCl fluid inclusions are relatively abundant in sample 89RAO42, where they occur along subvertical healed microfractures. As in fault veins, these inclusions have low eutectic temperatures (Figure 7) indicating the presence of $CaCl_2$ and other salts in addition to NaCl. Melting of salt hydrate or of ice occurs between -51.2°C and -2.4°C, and salinities of the aqueous fluid vary from one microcrack to the other (Figure 9d). Most H_2O-NaCl fluid inclusions have homogenization temperatures between 70 and 170°C, except for a few microcracks in which inclusions homogenize above 180°C (Figure 9d). Calculated salinities range from 4 to 30 wt % eq NaCl, corresponding to calculated densities of 580 to 1200 kg/m³.

H_2O-NaCl fluid inclusions are scarce in sample 89RAO44. Eutectic temperatures between -38°C and -32°C and ice melting temperature between -8°C and -2°C indicate more dilute aqueous fluids than in sample 89RAO42, and calculated salinities range from 1.7 to 12 wt % eq NaCl. The homogenization temperatures are relatively low (85-165°C) and correspond to densities of 950 to 1010 kg/m³.

Interpretation of Fluid Inclusion Data

Fluid inclusion results presented here for the Sigma mine indicate that three types of fluids were present during the development of QTC veins: CO_2-rich, H_2O-CO_2, and H_2O-NaCl fluids, consistent with results of previous studies on these veins [*Robert and Kelly*, 1987; *Guha et al.*, 1991; *Burrows and Spooner*, 1990] and of fluid inclusion studies in progress on three other deposit in the district. Coexisting CO_2-rich and H_2O-NaCl fluids were considered by *Robert and Kelly* [1987] to result from variable degrees of intermittent unmixing from an homogeneous parent H_2O-CO_2 fluid of low salinity infiltrating both vein types. This interpretation is further supported by the fact that H_2O-CO_2 inclusions in extensional veins homogenize to both liquid and vapor phases, as indicated above. *Guha et al.* [1991] further showed that in extensional veins H_2O-rich and CO_2-(CH_4)-rich fluids were trapped in separate inclusions, interpreted to be the result of unmixing, whereas a single parent homogeneous H_2O-CO_2-(CH_4) fluid was trapped in adjacent hydrothermally altered wall rocks. Such heterogeneous versus homogeneous fluid trapping has been interpreted to be triggered by fluctuations in fluid pressure between lithostatic and lower values during vein development [*Robert and Kelly*, 1987; *Sibson et al.*, 1988].

It should be noted that two groups of H_2O-NaCl fluid inclusions have to be distinguished: those with $T_h > 200$°C and those with $T_h < 180$°C (Figures 8c and 9d). Inclusions of the high-temperature group are interpreted to result from unmixing of the parent H_2O-CO_2 low salinity fluid and by mechanical separation from the coexisting carbonic phase due to their different wetting properties [*Watson and Brennan*, 1987]. Inclusions of the second group cannot be ascribed to such a process because of their low T_h and their high but variable salinities; their composition is similar to Canadian Shield basement brines that percolated down the crust [*Kyser and Kerrich*, 1990] and which may have been trapped in open vertical microcracks.

Given that the ambient wall rock temperature is unlikely to vary significantly during vein development, differences in fluid pressure at different stages in vein development should be

recorded as differences in densities of fluid inclusions trapped at such different stages. Thus, if no leakage of fluid inclusions occurs after trapping, fluid pressure fluctuations could be documented by comparing densities of a given type of fluid inclusion in different sites in a vein, such as between microcracks.

CO_2-bearing fluid inclusions within a number of clusters and microcracks, especially in extensional veins, show textural evidence for leakage and/or reworking as well as variations in the degree of filling and consequently in fluid density, ascribed in part to deformation of the host quartz crystal. These features may indicate that fluid inclusions evolved out of their isochoric line during their postentrapment history, as reproduced experimentally by *Pêcher and Boullier* [1984], *Boullier et al.* [1989], and *Sterner and Bodnar* [1989] or that preferential water loss from fluid inclusions occurred [*Bakker and Hansen*, 1991; *Hall and Sterner*, 1993]. This postentrapment evolution of fluid inclusions would preclude any calculation of fluid pressure using microthermometric data. However, the observed scattering of $T_h CO_2$ within single microcracks (up to 50°C, see Figure 9c) is much larger than that (< 10°C) attributed to postentrapment evolution in other studies [*Pêcher*, 1979; *Boullier et al.*, 1991; *Diamond*, 1990], suggesting that at least another phenomena is responsible for such large scattering of T_h.

We propose that within-crack variations in $T_h CO_2$ or in degree of filling may result from variations in fluid pressure during crack healing. The healing process of microcracks is a relatively rapid process (days to months) under the P-T conditions considered here [*Brantley*, 1992]. Given that significant variations in ambient T and confining P are unlikely in such a short time frame, within-crack variations of fluid inclusion densities most likely reflect local and relatively rapid variations in fluid pressure. The decelerating effect of CO_2 on the healing process [*Brantley*, 1992] could explain why $T_h CO_2$ are more scattered in microcracks containing CO_2-rich fluids compared to those containing H_2O-CO_2 fluids.

Thus variations in fluid densities between individual cracks and clusters within the same samples, and possibly within-crack variations, should reflect variations in fluid pressure. In order to determine fluid densites with sufficient accuracy for such comparisons, quantitative determination of the composition of the volatile phase (especially for CO_2-bearing fluid inclusions) is required. Such determinations on carefully selected fluid inclusions are currently underway using Raman spectroscopy. However, preliminary density calculations have been performed using fluid composition determined from microthermometric data; the calculated isochores for selected planes of both CO_2-rich and H_2O-CO_2 fluid inclusions are illustrated in Figure 11 for each sample. Although the absolute pressure values must be considered with caution, the ranges in trapping pressure indicated by both types of fluid inclusions are very significant. At a temperature of 350°C (selected on the basis of homogenization temperatures of H_2O-CO_2 inclusions), trapping pressures determined from CO_2-rich and H_2O-CO_2 fluid inclusions show a total range of 200 MPa (from 150 to 350 MPa) in both extensional vein samples and of 350 MPa (from 100 to 450 MPa) in the fault vein sample (Figure 11).

In summary, the preliminary fluid inclusion data presented above indicate significant fluctuations in fluid pressure during vein development, as suggested by *Robert and Kelly* [1987], *Sibson et al.* [1988], and *Boullier and Robert* [1992].

Model for Cyclic Vein Development

The structural attributes and relationships of QTC veins presented above clearly point to the sequential, cyclic development of reverse fault veins and extensional veins in alternating stages of growth and deformation. Fluid inclusion data further indicate that significant fluid pressure fluctuations
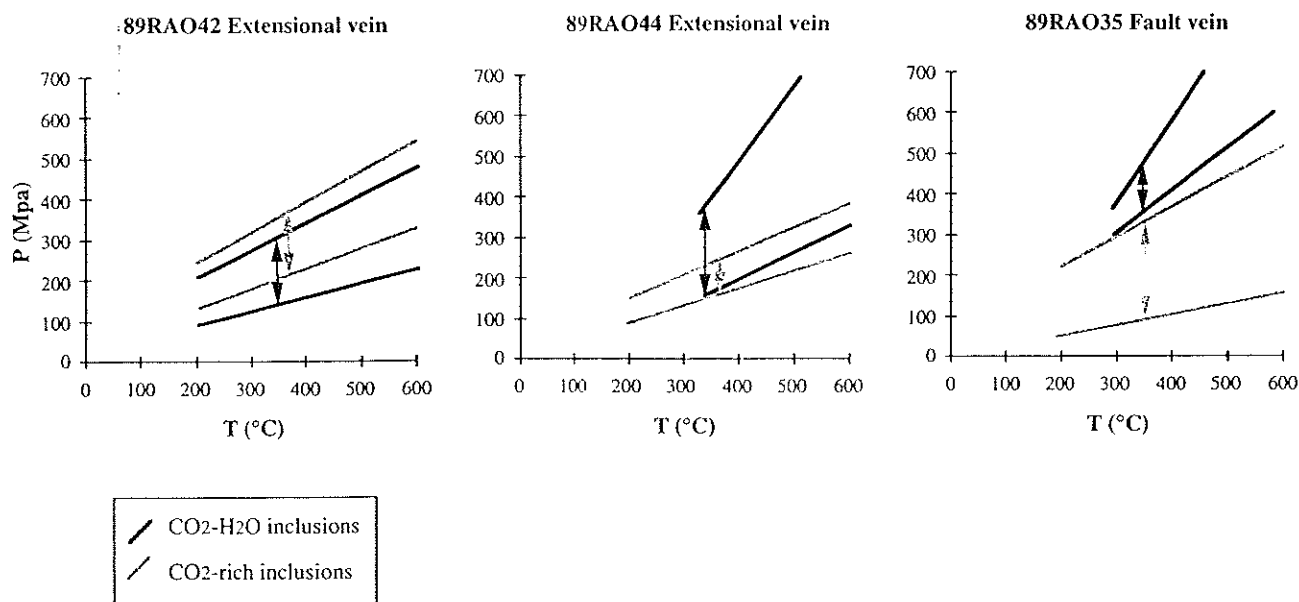

Figure 11. *P-T* diagram showing calculated isochores for selected planes of CO_2-rich and H_2O-CO_2 fluid inclusions in each of the three samples studied in detail. Arrows show the range in fluid pressure at a temperature of 350°C.

accompanied vein formation. It is important to emphasize here that the H_2O-CO_2-salt fluids responsible for mineralization were external to the volumes of rocks encompassing the QTC vein deposits and were not pore fluids within, and adjacent to, mineralized faults. This conclusion is supported by mass balance calculations on hydrothermally altered wall rocks, which show that CO_2 and large amounts of silica were introduced [*Robert and Brown*, 1986b], and by the deep crustal or upper mantle origin of at least some components of the fluids, including CO_2, as indicated by geochemical and isotopic tracers [*Kerrich and Wyman*, 1990; *Anglin*, 1992].

Cyclic vein development has been previously correlated with the earthquake cycle through the fault valve model [*Sibson et al.*, 1988; *Cox et al.*, 1991; *Boullier and Robert*, 1992; *Cox*, this issue], and we present here a more detailed four-stage model (Figure 12).

Stage 1: Preseismic Stage

This stage is characterized by increasing shear stress (τ) along the misoriented fault in a N-S compressional regime, with horizontal σ_1 and vertical σ_3 (Figure 12), and by increasing pressure of externally derived fluid along the fault, probably as a result of the ascent of a "fluid domain" along master faults and splays perhaps in the manner discussed by *Gold and Soter* [1985]. It results in the aseismic deformation

of fault veins and their host shear zones and in the development of subhorizontal extensional veins in isotropic rocks (hydraulic fractures) which requires conditions of near-lithostatic P_f and low differential stress (σ_1 - $\sigma_3 < 4T$ and $P_f > \sigma_3 + T$ [*Secor*,1965]). The existence of a sealed segment of a fault will impede the ascent of such fluid domains and will likely lead to dispersion and storage of fluids in subhorizontal hydraulic fractures developing in intact rocks on both sides of the fault, as proposed by *Cox* [this issue].

In fault veins, structures produced during this stage include stylolites with N-S horizontal peaks, and those indicating plastic deformation and dynamic recrystallization of quartz, all characteristics of aseismic deformation. The hydrothermal slicken fibers indicating reverse movement may have developed during this stage, or during a different part of the cycle (see below). In extensional veins, crack seal structures, subhorizontal fluid inclusion planes (healed microcracks), vertical tourmaline fibers, and open-space filling textures, indicating vein growth (Table 1), are attributed to this preseismic stage.

Two types of microcracks are preserved in extensional veins: those related to delicate crack seal layers and those that are healed microcracks marked by fluid inclusions. Crack seal structures, which are parallel to vein walls and follow their irregularities, have been interpreted as resulting from subcritical crack growth by *Cox* [1991] and by *Boullier and*
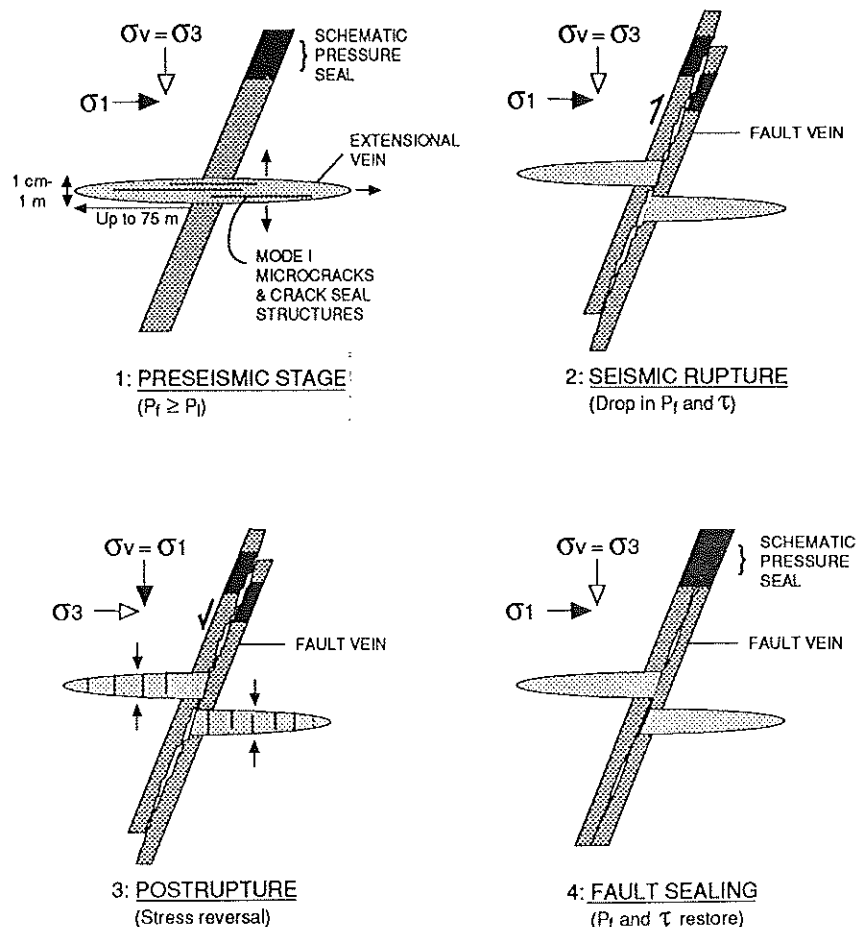

Figure 12. Diagram illustrating the main stages of vein development and selected microstructures in relation to the earthquake stress cycle. See text for explanations.

Robert [1992]. Such structures involve the input of matter from the infiltrating external fluid and contribute to vein growth. In contrast, healed microfractures parallel to vein walls are planar and more likely result from dynamic crack growth. They are self-healed microcracks involving dissolution-recrystallization processes and therefore do not involve external input of matter. The difference in propagation mode between the two types of wall-parallel fractures may reflect variations in driving pressure [*Pollard and Segall*, 1987; *Cox*, 1991] during this stage of the cycle.

Stage 2: Seismic Rupture Stage

Earthquake rupture along the fault occurs once τ reaches the appropriate level given the shear strength of the fault and the prevailing P_f. An important consequence of rupture is the breaching of the pressure seal and the consequent drop in P_f. This will trigger progressive drainage of the overpressured fluids upward along the fault, including fluids stored in hydraulic fractures that may be flushed back into the fault [*Cox*, this issue]. Seismic rupture may have produced the locally observed fault breccias with hydrothermal matrix along fault veins. Similarly, jigsaw puzzle breccias (Figure 4c) may represent implosion breccias formed in dilational jogs as a result of rupture and related sudden fluid pressure differentials [*Sibson*, 1986]. However, the occurrence of such breccias at dilational jogs has not been observed, perhaps because such jogs have been obscured by continued propagation and development of fault veins.

Another consequence of the drop in P_f is the interpreted unmixing of a parent H_2O-CO_2-salt fluid into immiscible H_2O-rich and CO_2-rich fluids, which may be physically separated into different sites and microcracks within the veins due to their different wetting properties [*Watson and Brennan*, 1987]. Rupture will also be accompanied by release of τ along the fault, which may enhance recrystallization of the internally and plastically deformed quartz crystals within fault veins.

Stage 3: Immediate Postrupture Stage

Several microstructures of extensional veins indicate vertical shortening of the veins, such as kinked vertical tourmaline fibers, vertical microcracks and horizontal boudinage (Table 1 and Figure 12). This vertical shortening requires a reversal of local vertical and horizontal principal stress axes [*Boullier and Robert*, 1992], which is interpreted here to take place immediately after rupture. Such transient stress reversal is conceivable when faulting occurs under the conditions of low differential stress required for the formation of extensional veins, as hydraulic fractures. It further requires total release of τ along the fault plane, perhaps with dynamic overshoot [*Sibson*, 1992]. The formation of hydrothermal slicken fibers of normal sense observed along some fault veins may be a consequence of overshoot. In instances where overshoot and stress reversal did not take place, development of slicken fibers of reverse sense may also have taken place during postseismic afterslip.

Stage 4: Fault Sealing Stage

Following the transient local stress reversal, far field stresses with horizontal σ_1 will begin acting on the fault again (Figure 12), along which τ will progressively restore.

The postrupture drop in P_f as well as the postrupture renewed ascent of deeper fluids along the now permeable fault, will likely promote precipitation of quartz, the solubility of which is pressure-sensitive under hydrothermal conditions considered here. Similarly, any fluid unmixing related to P_f drop will promote precipitation of carbonate within fault veins. Such mineral precipitation will induce a decrease in permeability of the fault and will lead to its sealing [*Sibson et al.*, 1988], which could be further assisted by dissolution-recrystallization processes within the veins and shear zones as shown by stylolite development [*Gratier et al.*, 1994]. As a consequence of fault sealing, the pressure of the externally supplied fluid will build up again, leading to repetition of the cycle.

Stages 1 and 4 of the above model are intimately linked because the development of extensional veins will depend in part on the relative rates of P_f and τ restoration, the degree of misorientation of the fault, and its cohesive strength [*Cox*, 1991; *Sibson*, 1992]. For example, if τ along the fault restores faster than P_f, then rupture may in some instances (depending on the degree of misorientation) occur along the fault before development of extensional veins. This may partly explain why fault veins in some deposits are not fringed by extensional veins, corresponding to cases of "minor valve action," in contrast to extreme fault valve behavior recorded in deposits containing well-developed horizontal extensional veins [*Sibson*, 1992].

According to this model, each recognizable quartz lamina within a fault vein should be the product of one cycle. Within fault veins, several tens (20-100) of laminae can commonly be identified. They provide a minimum estimate for the number of cycles, or earthquakes, involved in the formation of these veins, because individual quartz lamina not bounded by tourmaline-bearing surfaces will be very difficult to recognize (quartz against quartz) and because not all slip increments are likely to be accompanied by dilation and precipitation of quartz and carbonate.

Discussion

The four-stage model presented above for the development of QTC veins at Val d'Or hinges heavily on two points which deserve further consideration: supralithostatic, but fluctuating fluid pressures and seismic slip events within fault veins. As pointed out above, the development of subhorizontal extensional veins in intact rocks provides good evidence for the involvement of overpressured fluids ($P_f \geq P_l$) at least at some stage during the vein development cycle.

Perhaps one of the most convincing test of the fault valve model would be to document differences in trapping pressures (reflecting P_f fluctuations) of primary fluid inclusions between pairs of extensional and fault veins: primary fluid inclusions in quartz in extensional veins should be trapped at lithostatic pressures, whereas those in quartz within dilational parts of fault veins should be trapped at sublithostatic pressures (Figure 12). Studies to that effect are currently under way. However, it is a difficult task because the density and composition of fluid inclusions may be modified after trapping, as discussed above. Nevertheless, the documented ranges of fluid inclusion densities along different microfractures within the same sample corresponds to total pressure ranges, or fluctuations, of the order of 200 MPa in

extensional veins and of 350 MPa in fault veins, based on the preliminary calculations presented above.

Direct evidence for seismic slip within fault veins is scarce, perhaps because of a poor degree of preservation and because of the difficulty in distinguishing between the products of seismic and aseismic brittle-frictional sliding. However, discrete slip surfaces, submillimetric bands of very finely crushed tourmaline, and fault breccias with hydrothermal cement within and along fault veins are tentatively interpreted as recording seismic slip. Finally, the presence of jigsaw puzzle breccias, tentatively interpreted as implosion breccias, as well as the documented stress reversal and overshoot during vein development are best explained in terms of a sudden release of shear stress along a fault vein following an earthquake rupture, and the consequent P_f drop.

Accepting the proposed fault valve model and considering that crustal-scale faults like the LLCF are the main channelway for upward fluid migration, one can further explore links between vein formation and earthquake processes, at least in a preliminary way, and suggest additional studies of these veins which may shed light on the involvement of fluids in faulting.

Size of Fault Vein-Related Earthquake Ruptures

In considering the relationships to earthquake processes, one of the first questions that comes to mind is the size of earthquakes accompanying each seismic slip increment along a fault vein. A crude estimate can be obtained based on the existing relationship between earthquake magnitude and typical source parameters such as rupture area and amount of slip, as determined by *Sibson* [1989, Table 1] for earthquakes with "typical" shear stress drops of ~3 MPa. These parameters can be estimated for a small number of fault veins, assuming they were derived from such events.

Maximum rupture areas are constrained by the total dimensions of the third-order structures hosting fault veins, which fall in the range of 10^4-10^6 m^2. This is a maximum because any rupture is unlikely to occupy the full dimensions of the finite fault. Third-order structures and fault veins are low-displacement structures: based on a small number of adequately constrained cases, total offsets, including any prevein slip, range from 0.1 to 2 m along small, discrete faults to a maximum of 20-30 m along kilometer-scale ductile shear zones. Fault veins hosted in discrete faults without ductile components of deformation provide the most realistic estimates of vein-related total slip. Assuming seismic slip only, the amount of slip related to each cycle is obtained by dividing the total displacements by the number of slip increments recognized within fault veins. As previously pointed out, the minimum number of slip increments along fault veins typically ranges from 20 to 100. Combined with intermediate values of total displacement along small, discrete faults, this number of slip increments yield maximum displacements on the order of a few centimetres for each slip event.

Rupture parameters crudely estimated from the above constraints (i.e., a few centimeters of slip and rupture areas of 10^4-10^6 m^2) correspond to earthquakes of $4 > M > 3$ or less [cf. *Sibson*, 1989, Table 1]. Given that these rupture parameters represent maximum estimates, vein-related earthquakes are likely to have been of smaller magnitude. Clearly, additional studies of well exposed fault veins should aim at documenting the number of slip increments, the total offset along the vein,

and the dimensions of the host structure and those of individual quartz laminae.

QTC Vein Distribution Versus Earthquake Distribution

The inferred magnitudes of fault vein-related earthquakes are relatively small compared to those ($M > 6$) expected for large earthquakes nucleating near the base of seismogenic regime and rupturing the full extent of the seismogenic zone along lithospheric fault zones such as LLCF [*Sibson*, 1989]. The relationships between expected large earthquakes along first-order structures and the widely distributed, smaller vein-related earthquakes along subsidiary structures may shed light on the district scale circulation and redistribution of fluids in relation to seismic faulting, and this subject deserves further investigation.

The distribution of QTC veins within the vein field at Val d'Or (Figure 1) can be regarded as reflecting the distribution of small earthquake events, integrated during the lifetime of the hydrothermal system. The QTC veins at Val d'Or (Figure 1) form a field or cluster which is approximately 30 km long and 15 km across and which is located in the hangingwall of the LLCF (Figure 1). It is interesting to note that such dimensions compare very well with those of clusters of aftershocks following major ruptures along the San Andreas fault system, such as the Loma Prieta, California, earthquake of October 17, 1989, with a cluster approximately 40 km long and 5 km across [*McNutt*, 1990], or the Morgan Hill, California, earthquake of April 24, 1984, with a cluster approximately 40 km long and 13 km across [*Cockerham and Eaton*, 1987]. Furthermore, at least some of the aftershocks occurred along subsidiary structures in both examples. The magnitude of the fault vein-related earthquakes estimated above, $4 > M > 3$ or less, is also consistent with that of the majority of aftershocks.

The potential relationships between fault vein-related ruptures and those along the LLCF is worth pursuing, but it is only possible to offer speculations at this stage. One possibility is that the individual seismic slip events along fault veins correspond to aftershocks along subsidiary structures related to major ruptures along the LLCF. Another possibility is that the fault vein-related ruptures represent a precursory earthquake swarm reflecting development of a large zone of pressurized hydrothermal fluids prior to a large rupture along the LLCF (R. H. Sibson, personal communication, 1994), as documented before some large earthquakes [*Evison*, 1977, 1982].

Duration of the Cycle

Another important question to pursue in relation to the analogy between vein formation and earthquake processes is the duration of the cycle in the four-stage fault valve model presented above, for comparison with recurrence interval of large earthquakes along lithospheric faults and for understanding factors involved in sealing of faults.

Because stages 2 and 3 are expected to take place rapidly, the duration of the fault valve cycle could be approximated by that of stages 4 and 1, which effectively correspond to the interseismic period. This in turn will depend largely on the rates of fault sealing, of P_f buildup (after sealing), and of τ restoring. It is not possible to place adequate constraints on

the rates of these processes and we can only indicate some of the controlling factors. As pointed out above, large volumes of external fluids containing significant levels of dissolved silica and CO_2 are involved in vein development. As a result, the rate of fault sealing will depend largely on the volume of external fluid infiltrating the permeable fault after rupture, precipitating quartz and carbonate due to changing P-T conditions, rather than on other local processes such as pressure solution, important in other situations [Gratier et al., 1994]. After sealing, the rate of P_f buildup will depend mostly on the rate of supply and ascent of deeper fluids [Gold and Soter, 1985].

Perhaps the duration of stage 1 could be estimated by considering the time required for the development of those individual layers in extensional veins that are dominated by crack seal structures. As suggested by Cox [1991] and Boullier and Robert [1992], crack seal structures in such layers likely developed by subcritical crack growth. The kinetics of their formation is controled by the slowest of the following two processes: the velocity of subcritical crack propagation, for which experimental data are available [Atkinson and Meredith, 1987], and the rate of supply and precipitation of silica required to seal the cracks, which is unconstrained at present.

Conclusions

The QTC veins of the Val d'Or district provide good evidence that gold-quartz vein fields in deformed terranes are fossil products of cyclic and linked hydrothermal and seismic events. A preliminary comparison of vein-related parameters and earthquake rupture parameters reveals many similarities of scale, dimensions and processes. Such an approach is worth pursuing with further systematic quantitative documentation of the physical and structural aspects of the veins and their host structures, as well as with linked microstructural and fluid inclusion studies. Finally, it should be reemphasized that these vein fields offer excellent opportunities for exploring and studying in three dimensions and at different scales earthquake-related processes exhumed from the base of the seismogenic zone.

References

Anglin, C. D., Sm-Nd and Sr isotopic studies of scheelite from some Superior Province gold deposits, Ph.D. thesis, 219 pp., Carleton Univ., Ottawa, Ont., Canada, 1992.

Atkinson, B.K., and P. G. Meredith, The theory of sub-critical crack growth with applications to minerals and rocks, in Fracture Mechanics of Rocks, edited by B. K. Atkinson, pp. 111-166, Academic, San Diego, Calif., 1987.

Bakker, R. J., and J. B. H. Hansen, Experimental post-entrapment water loss from synthetic CO_2-H_2O inclusions in natural quartz, Geochim. Cosmochim. Acta, 55, 2215-2230, 1991.

Bodnar, R. J., Revised equation and table for determining the freezing point depression of H_2O-NaCl solutions, Geochim. Cosmochim. Acta, 57, 683-684, 1993.

Boullier, A. M., and F. Robert, Paloeseismic events recorded in Archean gold-quartz vein networks, Val d'Or Abitibi, Quebec, J. Struct. Geol., 14, 161-179, 1992.

Boullier, A. M., G. Michot, A. Pêcher, and O. Barrès, Diffusion and/or plastic deformation around fluid inclusions in synthetic quartz: New investigations, in Fluid Movements-Element Transport and the Composition of the Deep Crust, edited by D. Bridgwater, pp. 345-360, Kluwer Academic, Norwell, Mass., 1989.

Boullier, A. M., C. France-Lanord, J. Dubessy, J. Adamy, and M. Champenois, Linked fluid and tectonic evolution in the High Himalaya mountains (Nepal), Contrib. Mineral. Petrol., 107, 358-372, 1991.

Bozzo, A. T., H. S. Chen, J. R. Kass, and A. J. Bardhun, The properties of the hydrates of chlorine and carbon dioxide, Desalination, 16, 303-320, 1975.

Brantley, S. L., The effect of fluid chemistry on quartz microcrack lifetimes, Earth Planet. Sci. Lett., 113, 145-156, 1992.

Burrows, D. R., and E. T. C. Spooner, Archean intrusion-hosted, stockwork Au-quartz vein mineralization, Lamaque mine, Val d'Or, Quebec, Part I, Geologic and fluid characteristics, in Greenstone Gold and Crustal Evolution, NUNA Conference Volume, pp. 139-141, Geological Association of Canada, St. John's, Newfoundland, 1990.

Byerlee, J., Model for episodic flow of high-pressure water in fault zones before earthquakes, Geology, 21, 303-306, 1993.

Carmichael, D. M., Metamorphism, metasomatism, and Archean lode gold deposits, in Greenstone Gold and Crustal Evolution, NUNA Conference Volume, pp. 142-143, Geological Association of Canada, St. John's, Newfoundland, 1991.

Chen, H. S., The thermodynamics and composition of carbon dioxide hydrate, M.S. thesis, 67 pp., Syracuse Univ., Syracuse, New York, 1972.

Cockerman, R. S., and J. P. Eaton, The earthquake and its aftershocks, April 24 through September 30, U.S. Geol. Surv. Bull, 1639, 15-28, 1987.

Collins, P. L. F., Gas hydrates in CO_2-bearing fluid inclusions and the use of freezing data for estimation of salinity, Econ. Geol., 74, 1435-1444, 1979.

Corfu, F., The evolution of the Southern Abitibi greenstone belt in light of precise U-Pb geochronology, Econ. Geol., 88, 1323-1340, 1993.

Cox, S. F., Geometry and internal structures of mesothermal vein systems: Implications for hydrodynamics and ore genesis during deformation (extended abstract), in Structural Geology in Mining and Exploration, Publ. 25, pp. 47-53, University of Western Australia, Nedlands, 1991.

Cox, S. F., Faulting processes at high fluid pressures: - An example of fault valve behavior from the Wattle Gully fault Victoria, Australia, J. Geophys. Res., this issue.

Cox, S. F., M. E. Etheridge, and V.J. Wall, Fluid pressure regimes and fluid dynamics during deformation of low-grade metamorphic terranes: Implications for the genesis of mesothermal gold deposits, in Greenstone Gold and Crustal Evolution, NUNA Conference Volume, pp. 46-53, Geological Association of Canada, St. John's, Newfoundland, 1990.

Cox, S. F., V. J. Wall, M. E. Etheridge, and T. F. Potter, Deformational and metamorphic processes in the formation of mesothermal vein-hosted gold deposits- Examples from the Lachland fold belt in Central Victoria, Australia, Ore Geol. Rev., 6, 391-423, 1991.

Crawford, M. L., Phase equilibria in aqueous fluid inclusions, in Short course in fluid inclusions: Applications to petrology, edited by L. S. Hollister and M. L. Crawford, pp. 75-100, Mineralogical Association of Canada, Nepean, Ont., 1981.

Diamond, L. W., Fluid inclusion evidence for P-V-T-X evolution of hydrothermal solutions in late-Alpine gold-quartz veins at Brusson, Val d'Ayas, northwest Italian Alps, Am. J. Sci., 290, 912-958, 1990.

Eisenlohr, B. N., D. I. Groves, and G. A. Partington, Crustal-scale shear zones and their significance to Archean gold mineralization in Western Australia, Mineral. Deposita, 24, 1-8, 1989.

Etheridge, M. A., V. J. Wall, S. F. Cox, and R. H. Vernon, High fluid pressures during regional metamorphism and deformation: Implications for mass transport and deformation mechanisms, *J. Geophys. Res.*, *89*, 4344-4358, 1984.

Evison, F. F., The precursory earthquake swarm, *Phys. Earth Planet. Interi.*, *15*, 19-23, 1977.

Evison, F. F., Generalized precursory swarm hypothesis, *J. Phys. Earth*, *30*, 155-170, 1982.

Feng, R., and R. Kerrich, Single zircon age constraints on the tectonic juxtaposition of the Archean Abitibi belt and Pontiac Subprovince, Quebec, Canada, *Geochim. Cosmochim. Acta*, *55*, 3437-3441, 1991.

Feng, R., and R. Kerrich, ^{40}Ar-^{39}Ar age constraints on the thermal history of the Archean Abitibi greenstone belt and the Pontiac Subprovince: Implications for terrane collision, differential uplift, and overprinting of gold deposits, *Can. J. Earth Sci.*, *29*, 1389-1411, 1992.

Foxford, K. A., R. Nicholson, and D. A. Polya, Textural evolution of W-Cu-Sn-bearing hydrothermal veins at Minas da Panasqueira, Portugal, *Mineral. Mag.*, *55*, 435-445, 1991.

Gold T., and S. Soter, Fluid ascent through the solid lithosphere and its relation to earthquakes, *Pure Appl. Geophys.*, *122*, 492-530, 1985.

Gratier, J. P., Pressure solution-deposition creep and associated tectonic differentiation in sedimentary rocks, in *Deformation of Sediments and Sedimentary Rocks*, edited by M. E. Jones and R. M. F. Preston, *Geol. Soc. Spec. Publ. London*, *29*, 25-38, 1987.

Gratier, J. P., and J. F. Gamond, Transition betwen seismic and aseismic deformation in the upper crust, in *Deformation Mechanisms, Rheology and Tectonics*, edited by R. J. Knipe and E. H. Rutter, *Geol. Soc. Spec. Publ. London*, *54*, 461-473, 1989.

Gratier, J. P., T. Chen, and R. Hellman, Pressure solution as a mechanism for crack sealing around faults, in Proceedings of workshop LXIII: The Mechanical Involvement of Fluids in Faulting, *U.S. Geol. Surv.*, Open File Rep., 94-228, 279-300, 1994.

Green, A. G., B. Milkreit, L. J. Mayrand, J. N. Ludden, C. Hubert, S. L. Jackson, R. H. Sutcliffe, G. F. West, P. Verpaelst, and A. Simard, Deep structure of an Archean greenstone terrane, *Nature*, *344*, 327-330, 1990.

Guha, J., H.-Z. Lu, B. Dubé, F. Robert, and M. Gagnon, Fluid characteristics of vein and altered wall rock in Archean mesothermal gold deposits, *Econ. Geol.*, *86*, 667-684, 1991.

Hall, L. D., and S. M. Sterner, Preferential water loss from synthetic fluid inclusions, *Contrib. Mineral. Petrol.*, *114*, 489-500, 1993.

Heyen, G., C. Ramboz, and J. Dubessy, Simulation des équilibres de phases dans le système CO_2-CH_4 en dessous de 50°C et de 100 bar, *C. R. Acad. Sci.*, *294*, 203-206, 1982.

Hodgson, C. J., The structure of shear-related, vein-type gold deposits: A review, *Ore Geol. Rev.*, *4*, 231-273, 1989.

Jacobs, G. K., and D. M. Kerrick, Methane: an equation of state with application to the ternary system H_2O-CO_2-CH_4, *Geochim. Cosmochim. Acta*, *19*, 607-614, 1981.

Kerrich, R., Fluid infiltration into fault zones: Chemical, isotopic and mechanical effects, *Pure Appl. Geophys.*, *124*, 225-268, 1986.

Kerrich, R., and D. Wyman, Geodynamic setting of mesothermal gold deposits: An association with accretionary tectonic regimes, *Geology*, *18*, 882-882, 1990.

Kerrich, R., T. E. La Tour, and L. Willmore, Fluid participation in deep fault zones: Evidence from geological, geochemical, and ^{18}O/^{16}O relations, *J. Geophys. Res.*, *89*, 4331-4343, 1984.

Kyser, T. K., and R. Kerrich, Geochemistry of fluids in tectonically active crustal regions, in *Fluids in Tectonically Active Regimes of the Continental Crust*, *Short Course Handb.*, vol. 18, edited by B. E. Nesbitt, pp. 133-230, Mineralogical Association of Canada, Nepean, Ont., 1990.

McNutt, S., Loma Prieta earthquake, October 17, 1989, Santa Cruz County, California, *Calif. Geol.*, *43*, 3-7, 1990.

Parry, W. T., and R. L. Bruhn, Fluid pressure transients along seismogenic normal faults, *Tectonophysics*, *179*, 335-344, 1990.

Pêcher, A., Les inclusions fluides des quartz d'exsudation de la zone du MCT himalayen au Népal Central: Données sur la phase fluide dans une grande zone de cisaillement crustal, *Bull. Minéral.*, *102*, 537-554, 1979.

Pêcher, A., and A. M. Boullier, Evolution à pression et températures élevées d'inclusions fluides dans un quartz synthétique, *Bull. Minéral.*, *107*, 139-153, 1984.

Pollard, D. P., and P. Segall, Theoretical displacements and stresses near fractures in rocks: With applications to faults, joints, veins, dikes, and solution surfaces in *Fracture Mechanics of Rocks*, edited by B. K. Atkinson, pp. 277-349, Academic, San Diego, Calif., 1987.

Potter, R. W. I., and M. A. Clynne, Solubility of highly soluble salts in aqueous media, part I, NaCl, KCl, $CaCl_2$, $NaSO_4$ and KSO_4 solubilities to 100°C, *J. Res. U. S. Geol. Surv.*, *6*, 701-705, 1978.

Poulsen, K. H., and F. Robert, Shear zones and gold: Practical examples from the southern Canadian Shield, in *Mineralisation and Shear Zones*, *Short Course Notes*, vol. 6, pp. 239-266, edited by J. T. Burnsnall, Geological Association of Canada, St. John's, Newfoundland, 1989.

Powell, W. G., D. M. Carmichael, and C. J. Hodgson, Late-tectonic subgreenschist- to greenschist-facies metamorphism in the Duparquet-Rouyn area, southern Abitibi greenstone belt, in Abitibi-Grenville Transect, Rep. 33, pp. 47-52, LITHOPROBE Abitibi-Grenville Project, Montreal, Quebec, 1993.

Rice, J. R., Fault stress states, pore pressure distributions, and the weakness of the San Andreas fault, In *Fault Mechanics and Transport Properties in Rocks*, pp. 475-503, edited by B. Evans and T.-F. Wong, Academic, San Diego, Calif., 1992.

Robert, F., Structural setting and control of gold-quartz veins of the Val d'Or area, southeastern Abitibi Subprovince, in *Gold and Base Metal Mineralization in the Abitibi Subprovince, Canada, With Emphasis on the Quebec Segment*, Publ. 24, pp. 167-209, University of Western Australia, Nedlands, 1990.

Robert, F., Vein fields in gold districts: The example of Val d'Or, southeastern Abitibi subprovince, Quebec, in *Current Research 1994-C*, pp. 295-302, Geological Survey of Canada, Ottawa, Ont., 1994.

Robert, F., and A. C. Brown, Archean gold-bearing quartz veins at the Sigma mine, Abitibi greenstone belt, Quebec, part I, Geologic relations and formation of the vein system, *Econ. Geol.*, *81*, 578-592, 1986a.

Robert, F., and A. C. Brown, Archean gold-bearing quartz veins at the Sigma mine, Abitibi greenstone belt, Quebec, part II, Vein paragenesis and hydrothermal alteration, *Econ. Geol.*, *81*, 593-616, 1986b.

Robert, F., and W. C. Kelly, Ore-forming fluids in Archean gold-bearing quartz veins at the Sigma Mine, Abitibi greenstone belt, Quebec, Canada, *Econ. Geol.*, *82*, 1464-1482, 1987.

Scholz, C. H., Mechanics of faulting, *Annu. Rev. Earth Planet. Sci.*, *7*, 309-334, 1989.

Secor, D. T., Role of fluid pressure in jointing, *Am. J. Sci.*, *263*, 633-646, 1965.

Secor, D. T., Mechanics of natural extension fracturing at depth in the Earth's crust, *Geol. Surv. Can. Pap.*, *68-52*, 3-48, 1969.

Sibson, R. H., Brecciation processes in fault zones: Inferences from earthquake rupturing, *Pure Appl. Geophys.*, *124*, 159-175, 1986.

Sibson, R. H., Earthquake faulting as a structural process, *J. Struct. Geol.*, *11*, 1-14, 1989.

Sibson, R. H., Implications of fault-valve behavior for rupture nucleation and recurrence, *Tectonophysics*, *211*, 283-293, 1992.

Sibson, R. H., Load-strengthening versus load-weakening faulting, *J. Struct. Geol.*, *15*, 123-128, 1993.

Sibson, R. H., F. Robert, and K. H. Poulsen, High angle reverse faults, fluid-pressure cycling, and mesothermal gold-quartz deposits, *Geology*, *16*, 551-555, 1988.

Sterner, S. M., and R. J. Bodnar, Synthetic fluid inclusions. VII. Re-equilibration of fluid inclusions in quartz during laboratory. Simulated metamorphic burial and uplift, *J. Metamorph. Geol.*, *7*, 243-360, 1989.

Swanenberg, H. E. C., Phase equilibria in carbonic systems, and their application to freezing studies of fluid Inclusions, *Contrib. Mineral. Petrol.*, *68*, 303-306, 1979.

Vanko, D. A., R. J. Bodnar, and S. M. Sterner, Synthetic fluid inclusions: VIII, Vapor-saturated halite solubility in part of the system NaCl-CaCl$_2$-H$_2$O with application to fluid inclusions from oceanic hydrothermal systems, *Geochim. Cosmochim. Acta, 52*, 2451-2456, 1988.

Watson, E. B., and J. M. Brennan, Fluids in the lithosphere, 1. Experimentally determined wetting characteristics of CO$_2$-H$_2$O fluids and their implications for fluid transport, host-rock physical properties and fluid inclusion formation, *Earth Planet. Sci. Lett., 85*, 497-515, 1987.

Williams-Jones, A. E., and I. M. Samson, Theoretical estimation of halite solubility system NaCl-CaCl$_2$-H$_2$O : Applications to fluid inclusions, *Can. Mineral., 28*, 299-304, 1990.

Wilson, H. S., Lamaque mine, in *Structural Geology of Canadian Ore Deposits*, pp. 882-891, Canadian Institute of Mining and Metallurgy, West Montreal, Quebec, 1948.

Zhang, Y. G., and J. D. Frantz, Determination of the homogenization temperatures and densities of supercritical fluids in the system NaCl-KCl-CaCl$_2$-H$_2$O using synthetic Fluid inclusions, *Chem. Geol., 64*, 335-350, 1987.

A.-M. Boullier and K. Firdaous, C.R.P.G., CNRS, B.P. 20, 54501, Vandoeuvre-les-Nancy Cedex, France.

F. Robert, Geological Survey of Canada, 601 Booth St., Ottawa, Canada K1A 0E8. (e-mail: frobert@gsc.emr.ca)